

広島大学学術情報リポジトリ  
Hiroshima University Institutional Repository

Title	Structural implication for the impaired binding of W150A mutant LOX-1 to oxidized low density lipoprotein, OxLDL
Author(s)	Nakano, Shogo; Sugihara, Mamoru; Yamada, Risato; Katayanagi, Katsuo; Tate, Shin-ichi
Citation	Biochimica et Biophysica Acta - Proteins and Proteomics , 1824 (5) : 739 - 749
Issue Date	2012
DOI	<a href="https://doi.org/10.1016/j.bbapap.2012.02.003">10.1016/j.bbapap.2012.02.003</a>
Self DOI	
URL	<a href="https://ir.lib.hiroshima-u.ac.jp/00034810">https://ir.lib.hiroshima-u.ac.jp/00034810</a>
Right	(c) 2012 Elsevier B.V. All rights reserved.
Relation	



**Structural implication for the impaired binding of W150A mutant LOX-1 to oxidized low density lipoprotein, OxLDL**

荻Shogo Nakano, Mamoru Sugihara, Risato Yamada, Katsuo Katayanagi and  
Shogo Nakano, Mamoru Sugihara, Risato Yamada, Katsuo Katayanagi and  
Shin-ichi Tate\*

Department of Mathematical and Life Sciences,  
Graduate School of Science, Hiroshima University,  
1-3-1 Kagamiyama, Higashi-Hiroshima 739-8526, Japan

\*Corresponding author

Department of Mathematics and Life Sciences,  
Graduate School of Science,  
Hiroshima University  
1-3-1 Kagamiyama, Higashi-Hiroshima 739-8526, Japan

Tel/Fax: +81 82 424 7387

E-mail: [tate@hiroshima-u.ac.jp](mailto:tate@hiroshima-u.ac.jp)

## **ABSTRACT**

Lectin-like oxidized lipoprotein (OxLDL) receptor 1, LOX-1, is the major OxLDL receptor expressed on vascular endothelial cells. We have previously reported the ligand-recognition mode of LOX-1 based on the crystal structure of the ligand binding domain (C-type lectin-like domain, CTLD) and surface plasmon resonance analysis, which suggested that the functional significance of the CTLD dimer (the ‘canonical’ dimer) is to harbor the characteristic “basic spine” on its surface. In this study, we have identified the key inter-domain interactions in retaining the canonical CTLD dimer by X-ray structural analysis of the inactive mutant W150A CTLD. The canonical CTLD dimer forms through tight hydrophobic interactions, in which W150 engages in a lock-and-key manner and represents the main interaction. The loss of the Trp ring by mutation to Ala prevents the formation of the canonical dimer, as elucidated from docking calculations using the crystal structure of W150A CTLD. The results emphasize that the canonically formed CTLD dimer is essential for LOX-1 to bind to OxLDL, which supports our proposed view that the basic spine surface present in the correctly formed dimer plays a primal role in OxLDL recognition. This concept provides insight into the pathogenic pattern recognized by LOX-1 as a member of the pattern recognition receptors.

### *Keywords:*

C-type lectin-like domain, oxidized low density lipoprotein, atherosclerosis, receptor structure, pattern recognition receptor

## 1. Introduction

Serum low-density lipoproteins (LDLs) deposited in the artery wall are susceptible to oxidation. The oxidized form of LDL, OxLDL, activates immune systems and thus initiates pro-inflammatory cascade events leading to atherosclerosis [1, 2]. In the process, macrophages recruited to the artery wall rich in OxLDL uptake the modified lipoprotein, which subsequently induces chronic inflammatory events in atherogenesis [3, 4]. The atherosclerotic lesion consists of lipid-laden macrophages [5, 6]. The uptake of the oxidized lipoproteins by the immune cells is, therefore, recognized as the origin of atherogenesis. The OxLDL uptake is mediated by receptors located on the cell surface [7-12]. They are structurally distinct from the receptor for native LDL, the LDL receptor [13]. Macrophages in the lesions express various types of OxLDL receptors to phagocytize OxLDL generated in the artery wall [12].

The OxLDL receptors were originally identified as the receptors that bind and internalize OxLDL. Their binding specificities, however, are not limited to the OxLDL. They bind to a broad range of ligands, including apoptotic cells, anionic phospholipids, bacteria, amyloid, advanced glycation end-products (AGE) and other pathogen components [14]. These pathogenic ligands are scavenged through the internalization to the macrophages mediated by the receptors. Consequently, the receptors are called scavenger receptors (SRs) [7, 12, 14].

SRs are recognized as members of pattern recognition receptors that mediate innate immune host response through recognition of highly conserved pathogen-associated molecular patterns. SRs bind to endogenous neo-antigens in OxLDL through the recognition of their molecular patterns that are similar to those for microbial pathogen ligands. The accumulated evidence indicates that the activation of the innate immune system causes macrophage cholesterol loading and the subsequent chronic inflammatory cascade that leads to atherosclerosis [15].

The structurally unrelated SRs are classified into eight subclasses [12, 14]. Each member in the SRs should function as pattern recognition receptor in a similar manner but using different structural architectures. Detailed knowledge of how the receptor uses its molecular architecture to recognize pathogen patterns will facilitate research aimed at identifying the immune-active pathogenic patterns.

Lectin-like OxLDL receptor-1 (LOX-1) is a member of the SRs, belonging to Class E [14]. LOX-1 is the major OxLDL receptor on vascular endothelial cell, although it is also expressed on macrophages as the other SR [3, 9, 16, 17]. LOX-1 is also expressed on

smooth muscle cells that have migrated to atherosclerotic lesions [18]. LOX-1 mediated OxLDL uptake leads to dysfunctional endothelial cells, which is a pivotal step in the early stages of atherogenesis [17]. The dysfunctional endothelial cells facilitate the LDL deposition into the artery walls by loosening their cell-cell junctions and by recruiting monocytes that become macrophages in artery walls [3, 4]. The event finally results in the accumulation of the lipid-laden macrophage in the artery walls, which leads to the formation of the atherosclerotic plaque [16, 17]. Research indicates that vascular cell apoptosis is also mediated by LOX-1, which may cause atherosclerotic plaque rupture in the advanced stage of atherogenesis [19].

The pathological importance of LOX-1 is emphasized by recent *in vivo* experiments [20, 21]. LOX-1-null mice showed that LOX-1 expression promotes atherosclerotic plaque formation and development. On the other hand, mice that lack LOX-1 showed significantly reduced atherosclerotic plaque formation relative to the LOX-1 harboring counterpart that had the same genetic background except for the gene coding for LOX-1.

Among the OxLDL receptors, LOX-1 is one of the structurally well-characterized proteins. We previously reported the crystal structure of the ligand binding domain of LOX-1 and proposed its possible binding mode to OxLDL [22-24]. The ligand binding surface of LOX-1 has a characteristic basic-residue arrangement called as ‘basic spine’, which was shown to be responsible for OxLDL [22] (Fig. 1A). The basic spine presumably recognizes the negatively charged amphiphatic helices of ApoB-100, the proteinous component of LDL; at least nine 22-residue homologous amphiphatic helices are found in ApoB-100, which expose the negative charged surfaces to solvent upon binding to the lipid surface [3, 22].

Clustering on the cell surface is required for LOX-1 to specifically bind to OxLDL. The functional significance of LOX-1 clustering was shown by surface plasmon resonance (SPR) experiments and also through the OxLDL internalization assays using LOX-1 constitutively expressing cells [25, 26]. The single LOX-1 receptor exists as a homodimer with an inter-domain disulfide bond at C140 (Fig. 1B). The single receptor, however, does not show enough binding activity to OxLDL. This is a key difference from the ligand recognition of the LDL receptor; the single LDL receptor recognizes one native LDL particle [27]. LOX-1 may recognize the specific patterns present on the OxLDL surface in a multi-valent manner [3, 22, 25, 28].

We reported that a site-directed mutant LOX-1, W150A, severely reduces the binding activity to OxLDL [22]. In the crystal structure of LOX-1, W150 remains at a distal position from the binding surface harboring the basic spine (Fig. 1B). [22]. The SPR experiments also showed that a single dimeric W150A *per se* has little binding

activity [25]. NMR and CD spectral comparison between the wild-type and W150A LOX-1 ligand binding domain (C-type lectin-like domain, CTLD) showed that the W150A mutation caused no apparent structural changes [22]. The reduced binding of W150A LOX-1 can, therefore, be ascribed to other causes rather than large structural changes to CTLD.

Size-exclusion chromatography experiments showed that the W150A CTLD mutant has largely lost the ability to dimerize [25]. Since the monomeric form of the wild-type CTLD has negligible affinity to the modified LDL, as shown in the SPR experiments, the inactivity of the W150A mutant has been hypothesized to be caused by the reduced ability of the mutant protein to dimerize [25]. Even in the disulfide linked form, W150A CTLD may not be able to retain the proper dimer structure as observed for the wild-type protein. This observation suggests that the proper dimer form of CTLD is essential for the pathogen pattern recognition by LOX-1, probably mediated by the basic spine on the dimer surface.

In this study, we have solved the crystal structure of the W150A CTLD mutant to gain molecular insights into its impaired binding activity. The W150A CTLD structure compared with the wild-type CTLD dimer showed that there are key interactions required to stabilize the correct dimer form, namely the hydrophobic interactions mediated by residue W150 and the induced additional interactions mediated by residues H151 and Y197. The X-ray structure illustrates that the W150A mutation disables key inter-domain hydrophobic interactions, thereby also weakening the associated domain-domain interactions such that dimer formation is essentially lost. The inability of this mutant to form a dimer is likely to represent the reason why the mutant has lost the capacity to bind its cognate ligand, thereby supporting our postulate that the basic spine is functionally important in OxLDL binding [22].

## **2. Materials and methods**

### *2.1. Protein purification and crystallization*

LOX-1 is composed of four domains: the short cytoplasmic domain (residues 1–33), the trans-membrane domain (residues 34–60), the NECK domain that connects the trans-membrane domain and the ligand binding domain (residues 61–142) and the C-type lectin-like domain (CTLD) that functions as the ligand binding domain (residues 143–273) (Fig. S1). The NECK10-CTLD fragment construct contains the C-terminal ten

residues of the NECK domain (residues 133–273). The NECK10-CTLD includes residue C140 that forms the inter-domain disulfide bond.

The human LOX-1 W150A mutant NECK10-CTLD fragment comprising residues 133–273 was expressed as inclusion bodies in *E. coli* cells. The sample was refolded and purified according to a previously published procedure [25]. The correctly re-folded W150A NECK10-CTLD fragment present in the soluble fraction was purified as a His<sub>6</sub>-tagged protein by metal affinity chromatography with Talon Superflow (Chlontech). The N-terminal His<sub>6</sub>-tag was cleaved by PreScission protease (GE Healthcare), to leave a Gly-Pro-His-Met segment to the target construct. The protein loaded onto a gel filtration column to separate the monomer and dimer fragments; the applied sample (1.5 mg/ml) was eluted with the buffer solution (10 mM TrisHCl, pH 7.5) containing 400 mM NaCl. Despite the presence of C140, the majority of the W150A NECK10-CTLD protein eluted as a monomer (Fig. S2). For crystallization, the monomeric fragment was used. The W150A NECK10-CTLD crystals grew from an equal volume mixture of protein solution (5.0 mg/ml protein, 10 mM TrisHCl, pH 7.5 and 400 mM NaCl) and precipitant solution (20% PEG8000, 100 mM sodium citrate, pH 5.0, and 200 mM ammonium sulfate) at 277 K. The crystals were soaked into the cryo-protectant solution (30% PEG8000, 100 mM sodium citrate, pH 5.0, 200 mM ammonium sulfate and 20% PEG400) prior to data collection under N<sub>2</sub>-gas flow at 95 K. The data were collected at SPring-8 (BL38B1 beam-line) in Harima, Japan. The data were recorded on an ADSC Quantum 315 CCD detector and processed using the HKL2000/SCALEPACK software package [29]. In the early stage of the research, the crystal characterization was performed at the Photon Factory (BL5A beam-line) in Tsukuba, Japan.

The crystal structure of LOX-1 W150A NECK10-CTLD was determined at 2.3 Å resolution using the molecular replacement approach with the program Molrep [30] in the CCP4 suite [31]. The crystal structure of CTLD in the canonical dimeric form (PDB ID: 1YXK, chain A) was used as the template. The refinement and model building were done with the program Refmac [32] and Coot [33], respectively. The crystallographic parameters and statistics are summarized in Table 1. The structure coordinate was deposited to the Protein Data Bank (PDB ID: 3VLG).

## 2.2. NMR spectroscopy

Uniformly <sup>15</sup>N-labeled LOX-1 wild-type and W150A CTLD fragments (residues 143–273 with His<sub>6</sub>-tag at the N-terminus) were prepared using the refolding procedure presented above, in which the *E. coli* cells were grown in M9 minimal medium

containing  $^{15}\text{NH}_4\text{Cl}$ . The samples used in the NMR experiments included the His<sub>6</sub>-tag. Each fragment was dissolved in the solution containing 200 mM sodium acetate, pH 4.0. The sample concentration was adjusted to 0.2 mM. Two-dimensional (2D)  $^1\text{H}$ - $^{15}\text{N}$  HSQC spectra were collected at 25 °C on a Bruker DMX600 NMR spectrometer. All data were processed using the program NMRPipe [34] and spectra were viewed using NMRView [35]. The resonances assignments for the wild-type CTLD have previously been reported [28]. Assignment of the resonances arising from the W150A CTLD construct was made based on the proximity of each signal to the corresponding resonances acquired on the wild-type CTLD. This is because of the limited solubility of the mutant CTLD; the sample concentration was only 0.2 mM. Such a concentration prohibited the efficient acquisition of triple resonance experiments.

### *2.3. Assessment of CTLD dimer formation*

Dimer formation under neutral and acidic solution conditions were assessed by SDS-PAGE. The constructs used were the wild-type NECK10-CTL D and the W150A NECK10-CTL D constructs. The samples used were in the monomeric forms collected by gel filtration. . The collected fractions containing monomeric proteins were extensively dialyzed against a 200 mM sodium acetate buffer (pH 4.0) and were concentrated using a centrifugal concentrator device to give final sample concentrations of 1.5 mg/ml (wild-type) and 1.3 mg/ml (W150A mutant). The samples treated with  $\beta$ -ME and those in the non-reduced form were subjected to SDS-PAGE to measure the content of the disulfide-linked homo-dimer of the NECK10-CTL D fragment; the amount of the disulfide-linked dimer represents the ability of CTL D to self associate. The sample concentration was estimated by UV absorbance with the absorption coefficients calculated from the primary sequence:  $\epsilon_{280}$  for the wild-type and W150A were  $41820 \text{ M}^{-1} \text{ cm}^{-1}$  and  $36130 \text{ M}^{-1} \text{ cm}^{-1}$ , respectively [36].

### *2.4. Dimer stability elucidation from docking calculations with the X-ray structure of CTL D*

The probable dimer models were constructed using the W150A CTL D crystal structure and the program HADDOCK [37, 38]. The contact residues found in the wild-type homodimer structure (PDB ID: 1YXK) were used as ‘active’ residues in the input for the HADDOCK calculation. The active residues were treated to be in contact with each other in the HADDOCK calculation, where these residues were spatially

constrained by pseudo potentials to maximize the contact area among the residues selected. In this work, the residues were W150, P143, C144, P145 and Q146. In the calculation, ‘passive’ residues, whose structures are allowed to be changed in generating the docked structure, were automatically selected around the ‘active’ residues by the program. All calculation were done on the HADDOCK server [37].

### 3. Results

#### 3.1. Overall structure description of LOX-1 W150A CTLD

LOX-1 W150A NECK10-CTLD was crystallized in the monomeric form. In the W150A NECK10-CTLD crystal structure, only the segment ranging from residues 143 to 268 was observed, which corresponds to the core part of the CTLD. Although residue C140 was present, the protein was solved in the monomeric form. This is consistent with the result from the size exclusion analysis that showed that W150A CTLD has a lower ability to self-assemble when compared to the wild-type protein (Fig. S2).

The wild-type CTLD (residues 143–273, without C140), was crystallized as a dimer with ethylene glycol involved at the interface (PDB ID: 1YXJ) (Fig. S3A). The domain arrangement for the wild-type CTLD was different from that in the NECK14-CTLD structure with the inter-domain disulfide bond, i.e., the ‘canonical’ dimer that exerts OxLDL binding (PDB ID: 1YXK) (Fig. 1A). The residues, which are embedded at the dimer interface in the canonical dimer of the wild-type NECK14-CTLD, are not in contact in the wild-type CTLD ‘non-canonical’ dimer (Fig. S3A). Because there is no direct contact between the CTLDs in the non-canonical dimer is, thus, the structure should be recognized as the monomeric form of the wild-type CTLD.

In the following text, the wild-type CTLD in the ‘non-canonical’ dimer is referred to as the monomeric wild-type CTLD with the abbreviation of mCTLD<sup>wt</sup>. The CTLD in the canonical dimer is referred to as the dimeric wild-type CTLD, abbreviated as dCTLD<sup>wt</sup>. The W150A NECK10-CTLD protein that crystallized as monomer is referred to as mCTLD<sup>w150a</sup>.

The mCTLD<sup>w150a</sup> structure shows overall similarity to those of dCTLD<sup>wt</sup> and mCTLD<sup>wt</sup> (Fig. 2A). The backbone structure around Y197 showed significant differences among the three CTLD structures (Fig. 2B). It is remarkable that there are rather small backbone structural changes among the three proteins near the mutation site (Fig.2A).

The side-chain orientations of H151 and Y197 in both the monomeric CTLDs, including mCTLD<sup>w150a</sup> and mCTLD<sup>wt</sup>, were different from those in the dimeric form,

dCTLD<sup>wt</sup> (Fig. 2B). In the monomeric mCTLD<sup>wt</sup> and mCTLD<sup>w150a</sup>, the regions around Y178 and H151 are not located at the inter-domain contacts in the crystals, whereas they are buried in the canonical dimer structure (Fig. 2B). Those side-chain reorientations may be caused by their release from the inter-domain contact.

### *3.2. Change in the inter-domain hydrophobic contact by the W150A mutation*

W150 engages in tight inter-domain hydrophobic interactions in the canonical dimer (Fig. 3A). The aromatic ring of W150 is buried in the hydrophobic pocket in a lock-and-key fashion: the pocket contains the residues P143, C144, P145 and Q146 in the other chain and P143 in the same chain (Fig. 3A). The hydrophobic interactions form a trunk-shaped structure, which stabilizes the dimer (Figs. S3B and S3C).

The structure of mCTLD<sup>wt</sup> was overlaid onto each CTLD in the canonical dimer (Fig. 2B). The structure of the hydrophobic pocket is retained in mCTLD<sup>wt</sup>, which should allow similar inter-domain interactions as observed in the canonical dimer (Fig. 3B); the slight change in the side-chain orientation of Q146 in this putative dimer can be explained by the lack of contact with the W150 ring moiety.

As seen in the canonical dimer, the disulfide bond involving C140 is located in the flexible linker. The disulfide bond functions to confine the CTLDs to a limited conformational space; however, the bond *per se* does not seem to stabilize the canonical dimeric form because it stays in a relatively unstructured part (Fig. S3B). The trunk structure including the inter-domain hydrophobic interactions should have a primary role in making the canonical dimer (Fig. S3C).

The putative dimer was built with the mCTLD<sup>w150a</sup> structure overlaid onto the CTLDs in the canonical dimer (Fig. 3C). In mCTLD<sup>w150a</sup>, the structure of the hydrophobic pocket was disrupted, giving rise to a shallow cavity (Fig. 3C). Apparent side-chain reorientation of P143 may be caused by the loss of the intra-chain interaction with the tryptophan ring (Fig. 3C). Besides the loosening of the hydrophobic pocket, the smaller A150 hydrophobic moiety cannot facilitate the intimate inter-chain hydrophobic interactions as found in the canonical dimer (Fig. 3C). The structure explains that the W150A mutation does not retain the canonical dimer due to the loss of the inter-chain hydrophobic trunk.

### *3.3. Change in the inter-domain hydrogen bonding mediated by H151*

In the canonical dimer, H151 forms an inter-domain hydrogen bond with D147 (Fig.

4A). The hydrogen bonds may further stabilize the canonical dimer synergistically with the hydrophobic trunk formation.

In the mCTL<sup>D</sup><sup>wt</sup> structure, the H151 hydrogen bonds to D187 in the same chain (Fig. 4B). In the putative dimer built with mCTL<sup>D</sup><sup>wt</sup>, H151 is positioned to allow the inter-chain hydrogen bond to D147 by a slight side-chain flip (Fig. 4B). This suggests that the inter-chain hydrogen bond involving H151 is induced upon dimerization, and this is primarily mediated by the trunk hydrophobic interactions.

The intra-chain hydrogen bonding between H151 and D187 was also found in the mCTL<sup>D</sup><sup>w150a</sup> construct (Fig. 4C). As in the case for mCTL<sup>D</sup><sup>wt</sup>, the region around H151 is not in contact with the other chain in the crystal. In the putative mCTL<sup>D</sup><sup>w150a</sup> dimer, the slight flip of H151 and also D147 side-chains may facilitate the inter-chain hydrogen bonds (Fig. 4C). The intra-chain hydrogen bond between H151 and D187 was found in both the monomeric CTL<sup>D</sup>s, mCTL<sup>D</sup><sup>wt</sup> and mCTL<sup>D</sup><sup>w150a</sup>. The regions around H151 in the monomeric CTL<sup>D</sup>s are not in contact with the other domains in their crystals. The intra-chain hydrogen bond, therefore, must be the intrinsic form in the monomeric CTL<sup>D</sup>.

### *3.4. Change in the inter-chain hydrophobic interactions mediated by Y197*

In the canonical dimer, Y197 forms additional inter-chain hydrophobic interactions with the Phe-cluster consisting of F158, F200 and F202 (Fig. 5A).

In the modeled dimer using mCTL<sup>D</sup><sup>wt</sup>, Y197 is not juxtapositioned to the Phe-cluster (Fig. 5B). The Phe-cluster retains a similar backbone structure as in the canonical dimer. However, the F200 ring flips and blocks the engagement of Y197 into the pocket (Fig. 5B). Moreover, in the modeled dimer, the ring of F200 sterically clashes with Y197 (Fig. 5B).

The model dimer with mCTL<sup>D</sup><sup>w150a</sup> also showed that Y197 is out of the Phe-cluster as in the case for mCTL<sup>D</sup><sup>wt</sup> (Fig. 5C). The flipped ring of F200 prohibits the access of Y197 into the cluster, as was the case for mCTL<sup>D</sup><sup>wt</sup>.

In the model dimers of mCTL<sup>D</sup><sup>wt</sup> and mCTL<sup>D</sup><sup>w150a</sup>, only minor changes in the Y197 and F200 ring orientations were observed. As postulated for the H151 mediated hydrogen bond, the Y197 hydrophobic interaction may also happen synergistically upon dimerization through the trunk hydrophobic interactions mediated by W150.

### *3.5. Structural differences between the wild-type CTL<sup>D</sup> and W150A CTL<sup>D</sup> in solution*

Structural comparison between mCTL<sup>D</sup><sub>w150a</sub> and dCTL<sup>D</sup><sub>wt</sub> has shown that the W150A mutation disrupted the trunk hydrophobic interactions without leading to large backbone structure changes (Fig. 3C). To confirm the limited backbone structural changes by the mutation, we compared 2D <sup>1</sup>H-<sup>15</sup>N HSQC spectra between the isolated CTL<sup>D</sup>s of the wild-type and W150A mutant (Fig. 6A). This experiment was performed to determine whether any crystal packing effects artificially fix the CTL<sup>D</sup> in a particular conformation. Because of the limited solubility of the wild-type CTL<sup>D</sup>, only a selected number of the resonances were assigned [28]. The backbone resonance assignment was done on the wild-type CTL<sup>D</sup> at 0.5 mM concentration; under the concentration, the self-association of the CTL<sup>D</sup> made the signals from the residues in the canonical dimer interface severely broadened to prohibit their assignment, although the signals were well resolved for the sample at 0.1 mM concentration [28]. Because of the experimental limitation associated with the bad behaving character of the CTL<sup>D</sup> as NMR sample, the assignment remained incomplete. The solubility of the W150A mutant CTL<sup>D</sup> was substantially low; the preparable protein concentration was limited up to 0.2 mM. Thus, the triple-resonance based assignment was not allowed for the W150A CTL<sup>D</sup>. Although the resonance assignments were incomplete, we found that the spectral changes were localized around the mutation site, W150 (Figs. 6B and 6C).

The residues engaged in the hydrophobic interactions, including Y197, were not assigned due to line-broadening in the wild-type CTL<sup>D</sup> (Fig. 6B). The exception was F158 which was assigned under the conditions used. Spectral changes for the residues surrounding the hydrophobic interactions by Y197 were marginal: F158 in the Phe-cluster showed marginal spectral changes by the mutation and most residues out of the dimer interface showed small spectral changes. The spectral comparison is consistent with the X-ray structural differences showing the limited backbone changes in the Phe-cluster and its neighboring parts including the ligand binding surface.

The NMR observations confirmed that the backbone structural changes are restricted to regions adjacent to and including the trunk hydrophobic interaction site. The W150A mutation does not disrupt the ligand-binding surface structure, but it limitedly affects the inter-domain interface.

### *3.6. Plausible inter-domain contacts mediated by A150 elucidated by the docking calculations*

The putative dimer model using mCTL<sup>D</sup><sub>w150a</sub>, which is based on the canonical dimer structure of the wild-type NECK14-CTL<sup>D</sup>, demonstrated that the W150A mutant

has lost key inter-domain interactions mediated by the W150 ring (Fig. 3). To gain structural insights into the impaired dimerization of the W150A CTLD, we tried to model the possible dimer structures using docking calculation with the mCTLD<sup>w150a</sup> structure. In modeling the putative dimers of the W150A CTLD, we may expect for seeing the possibility of the canonical dimer formation by the W150A CTLD. We applied the docking simulation program HADDOCK to derive the model structures [38].

### *3.6.1. Dimer reconstruction using the dCTLD<sup>wt</sup> structure and the program HADDOCK*

To elucidate the validity of the dimer modeling using HADDOCK, a limited number of key inter-domain interactions were considered and we reconstruct the canonical dimer using the dCTLD<sup>wt</sup> coordinates. In the HADDOCK calculations, we assumed that the interactions among the residues found in the trunk structure are important in stabilizing the canonical dimer (Fig. 3): the residues P143, C144, P145, Q146 and W150 were considered to be in contact with each other, and therefore these residues were allowed to undergo small structural changes in adopting the docked dimer structure.

The HADDOCK calculations reproduced the canonical dimer as the most probable structure assuming the above residues are in contact (Fig. 7A). In the modeled dimer structure, the W150 mediated trunk hydrophobic interactions are reproduced (Fig. 7A). The associating inter-domain interactions mediated by residues H151 and Y197 were also reproduced in the HADDOCK model, even though their interactions are not assumed in the calculation. The reported energies for a cluster of the most probable model structures by HADDOCK are listed in Table 2.

### *3.6.2. Modeling the possible W150A CTLD dimers*

The docking calculation with HADDOCK, which successfully reproduced the canonical dimer, was applied to model the W150A CTLD dimer using the mCTLD<sup>w150a</sup> coordinates. In contrast to the case of dCTLD<sup>wt</sup>, the W150A CTLD dimer models did not converge with significant variability, and the backbone root-mean-square-deviation (rmsd) of the structures in the most probable structure cluster was much larger than the corresponding value for the wild-type (Table 2).

The two lowest scored structures are presented (Figs. 7B and 7C). The domain arrangements of the modeled structures are compared with that in the canonical dimer to show their structural gaps (Figs. S4). The modes of the residue contacts are different between the two dimers. The methyl group of A150 is too small to be embedded in a

hydrophobic pocket, and, thus, it is modeled to be merely associated with the clustered residues (Figs. 7B and 7C). In contrast to the wild-type dimer reconstruction, the W150A mutant allows various contacts of the hydrophobic residues at the interface (Figs. 7B and 7C). The docking calculation indicates that W150A CTLD forms different dimer conformations with similar stabilities, and all these conformations differ from the canonical form. This should indicate that the W150A CTLD loses the ability in forming the stable dimer. This is also suggested by the much increase in the number of the HADDOCK score for the W150A CTLD dimer, which indexes the relative stabilities among the docked model structures (Table 2) [38].

### *3.6.3. Surface structural changes caused by the W150A mutation*

The ligand binding surface structures of the probable W150A dimers were compared with that of the wild-type (Fig. 8). We previously reported that the LOX-1 ligand binding surface in the canonical dimer has the ‘basic spine’ on the hydrophobic surface, which is essential for OxLDL binding (Fig. 8A).

The modeled W150A dimers showed apparent domain rearrangements when compared to the canonical dimer, which led to surface structural changes (Figs. 8B and 8C). In the two representative model dimers, the surface charge distributions are much different from that in the canonical dimer. Both models have enhanced positive charges on the less hydrophobic area. The characteristic ‘basic spine’ structure is lost in the dimer models, which explains the drastic reduction in the OxLDL binding activities for the W150A mutant LOX-1 protein (Fig. 8)

## **4. Discussion**

### *4.1. Structural basis for the impaired activity of the W150A LOX-1 protein*

The present work demonstrated that the W150A LOX-1 mutant loses the key inter-domain hydrophobic interactions mediated by the W150 ring, and thus hampers the canonical dimer formation that is essential for OxLDL binding. Structural comparison of mCTLD<sup>w150a</sup> with the wild-type CTLDs, including mCTLD<sup>wt</sup> and dCTLD<sup>wt</sup>, identified the inter-domain interactions engaged in forming the canonical dimer. These key interactions include the inter-domain contacts mediated by the residues of H151 and Y197, in addition to the trunk hydrophobic interactions facilitated by W150 (Fig. 9A). In the canonical dimer, all of the interactions should cooperatively

stabilize the dimer (Fig. 9A). The structural comparison also suggested that the lack of the key inter-domain interactions, in which W150 is embedded in a lock-and-key manner, results in a loss of all inter-domain interactions (Fig. 9B). The possible dimer structures formed by W150A CTLDs, which were modeled from the docking calculations, do not form the canonical dimer. They have disarranged dimers that do not retain the 'basic spine' structure. The modeled structures provide insight into the drastic loss of OxLDL binding of the W150A LOX-1 mutant.

#### *4.2. Stabilization of the canonical CTLD dimer in the extracellular part of LOX-1*

The extracellular part of LOX-1 consists of the NECK domain and the CTLD. The NECK facilitates dimer formation through its coiled-coil structure that promotes dimerization. In human LOX-1, the homodimeric architecture of the extracellular part is further stabilized by the inter-chain disulfide bond at C140. This disulfide-bond is, however, known to be non-essential in LOX-1 function and the cysteine is not conserved in the other LOX-1 orthologs.

The NECK domain confines the CTLDs in a limited space. The wild-type CTLDs in the confined space should autonomously form the canonical dimer through inter-domain interactions, in which the hydrophobic interactions mediated by W150 play a key role (Fig. 9A). The W150A mutant does not form the canonical dimer, even when the CTLDs are in spatial proximity through the dimerization of the NECK domains (Fig. 9B).

Using gel filtration chromatography, the W150A mutant CTLD has been previously shown to have a reduced ability to form a dimer [25]. In preparing the W150A NECK10-CTLTD fragment, only 14% of the protein is purified as the disulfide linked dimer. This is contrast to that for the wild-type NECK10-CTLTD, where 75% of the fragment formed the disulfide-linked dimer [25]. This significant difference in dimer formation represents the reduced self-assembling ability of the W150A CTLD. This may indicate that the W150A CTLD does not maintain the canonical dimer even in the disulfide-linked form, and, thus, it cannot keep the basic spine structure, which may explain our previous result that the disulfide-linked W150A CTLD has no apparent affinity to the ligand [25].

#### *4.3. pH effect on the dimerization of CTLD*

The wild-type CTLD showed two different dimer forms in the crystal [22]. The CTLD fragment without C140 (residues 143–273) formed the non-canonical dimer,

whereas the NECK14-CTLD (residues 129–273) formed the canonical dimer with the disulfide-linkage at C140. The primary cause for this observation must be ascribed to the lack of the inter-domain disulfide bond at C140 in the CTLD fragment, which enables the CTLDs to form the canonical dimer. pH may also play a role in facilitating dimer formation.

In crystallizing the CTLD fragment without C140, the solution was acidic, pH 5.0, whereas the NECK14-CTLD construct was crystallized at a near neutral solution, pH 7.5. To observe the pH effect on dimer formation, we compared the dimerization efficiencies for the wild-type and W150A NECK10-CTLD fragments. For the experiment on the wild-type NECK10-CTLD fragment, the monomeric fragment collected in the gel filtration analysis was used.

The dimerization efficiency was compared with the amount of the disulfide-linked dimer by SDS-PAGE (Fig. S5). The result demonstrated that the wild-type NECK10-CTLD dimerization efficiency was significantly reduced in the acidic environment relative to that at neutral pH (Fig. S5A). The non-canonical dimer formation of the wild-type CTLD lacking C140 may be partly ascribed to the reduced ability of the CTLD to self-associate under acidic conditions in addition to the absence of the disulfide bond which restricts the spatial position of the CTLDs.

In the case of the W150A NECK10-CTLD fragment, no dimer was observed under both neutral and acidic conditions (Fig. S5A). This result indicates that the W150A NECK10-CTLD was crystallized as a monomer because of the loss of intrinsic dimerization ability and this was apparently independent of the pH.

Endosomes are known to maintain an acidic internal pH [39]. The reduced dimerization ability of the wild-type CTLD under acidic conditions may suggest that the internalized LOX-1 in endosomes may disorganize the CTLDs and thus release OxLDL. This postulate is consistent with the proposed ligand releasing mechanism of the native LDL receptor in the endosome. Here, release of LDL is believed to be regulated by a pH-induced domain rearrangement under the acidic internal pH of the endosome [27].

## 5. Conclusion

In this study, the inter-domain interactions essential for the canonical dimerization of LOX-1 were identified based on the crystal structure of the W150A mutant. Residue W150 functions in a lock-and-key manner to inter-lock two CTLDs to form the functional dimer. The W150A mutation disrupts the canonical dimer due to the loss of key inter-domain interactions and thus disrupts the ‘basic spine’ on the ligand binding

surface, which explains the impaired binding activity of the mutant. The results highlight the functional importance of the basic spine structure in the binding of OxLDL.

The extra-cellular part of LOX-1 consists of the coiled-coil NECK and the CTLD. The CTLDs in the extra-cellular part are confined to a limited space because of the dimerized NECK domain. The reduced ability in the self-association of the W150A CTLD does not form the canonical dimer even in the presence of the dimerized NECK. NECK dimerization *per se* does not stabilize the CTLD dimer in the functionally active canonical form, although it facilitates the CTLD dimerization; the wild-type CTLD has the ability to autonomously form the canonical dimer, thus, the NECK prompts it. The self-assembling feature of the CTLD is the key to retain the active dimeric form of the LOX-1 ligand binding part.

CTLD self-assembly was shown to be pH-dependent; the wild-type CTLD showed reduced dimerization under acidic conditions. This reduction may be related to the inter-domain interaction mediated by His151; the protonation to the histidine should prohibit the inter-domain hydrogen bonding. This suggests that the internalized OxLDL should be released from LOX-1 due to the reduced dimer stability in the endosome, which has an acidic interior [27]. Further quantitative characterization of the CTLD dimerization in various environmental conditions remains to be completed.

Overall, this study has emphasized the functional importance of the self-assembling feature associated with the CTLD to retain the canonical dimer through the specific inter-domain interactions; the canonical dimer form is required to exert OxLDL binding activity *via* the basic spine on the dimer surface.

## **Acknowledgments**

The authors appreciate the technical assistance provided by Mr. Hirokazu Amida during the early stages of this work. This work was supported by a grant-in-aid for scientific research (B) (20390012) from the Japan Society for the Promotion of Science (JSPS). Part of the work was supported by a grant-in-aid for scientific research on the priority area “Molecular Science for Supra Functional Systems” (no. 19056009) from the Ministry of Education, Culture, Sports, Science and Technology (MEXT), Japan. The X-ray data collections were carried out at the SPring-8 using the BL38B1 beam-line (research proposal no. 2010B1666) and the Photon Factory using the BL5A beam-line (research proposal no. 2010U002). The authors acknowledge the support from the staff at the SPring-8 and the Photon Factory for their technical assistance.

## References

- [1] P. Holvoet, G. Perez, Z. Zhao, E. Brouwers, H. Bernar, D. Collen, Malondialdehyde-modified low density lipoproteins in patients with atherosclerotic disease, *The Journal of clinical investigation*, 95 (1995) 2611-2619.
- [2] P. Holvoet, Oxidative modification of low-density lipoproteins in atherothrombosis, *Acta cardiologica*, 53 (1998) 253-260.
- [3] S. Tate, Structure and mode of ligand recognition of the oxidized LDL receptor, LOX-1, in: K. Morikawa, S. Tate (Eds.) *Functional and Structural Biology on the Lipo-network*, Transworld Research Network, Kerala, India, 2006, pp. 179-198.
- [4] T. Kita, N. Kume, M. Minami, K. Hayashida, T. Murayama, H. Sano, H. Moriwaki, H. Kataoka, E. Nishi, H. Horiuchi, H. Arai, M. Yokode, Role of oxidized LDL in atherosclerosis, *Annals of the New York Academy of Sciences*, 947 (2001) 199-206.
- [5] R.G. Gerrity, H.K. Naito, Lipid clearance from fatty streak lesions by foam cell migration, *Artery*, 8 (1980) 215-219.
- [6] R.G. Gerrity, H.K. Naito, Ultrastructural identification of monocyte-derived foam cells in fatty streak lesions, *Artery*, 8 (1980) 208-214.
- [7] Y. Yamada, T. Doi, T. Hamakubo, T. Kodama, Scavenger receptor family proteins: roles for atherosclerosis, host defence and disorders of the central nervous system, *Cellular and molecular life sciences : CMLS*, 54 (1998) 628-640.
- [8] U.P. Steinbrecher, Receptors for oxidized low density lipoprotein, *Biochimica et biophysica acta*, 1436 (1999) 279-298.
- [9] T. Sawamura, N. Kume, T. Aoyama, H. Moriwaki, H. Hoshikawa, Y. Aiba, T. Tanaka, S. Miwa, Y. Katsura, T. Kita, T. Masaki, An endothelial receptor for oxidized low-density lipoprotein, *Nature*, 386 (1997) 73-77.
- [10] M.W. Freeman, Scavenger receptors in atherosclerosis, *Current opinion in hematology*, 4 (1997) 41-47.
- [11] B.S. Dhaliwal, U.P. Steinbrecher, Scavenger receptors and oxidized low density lipoproteins, *Clinica chimica acta; international journal of clinical chemistry*, 286 (1999) 191-205.
- [12] K.J. Moore, Scavenger Receptors in Atherosclerosis: Beyond Lipid Uptake, *Arteriosclerosis, Thrombosis, and Vascular Biology*, 26 (2006) 1702-1711.
- [13] G. Rudenko, L. Henry, K. Henderson, K. Ichtchenko, M.S. Brown, J.L. Goldstein, J. Deisenhofer, Structure of the LDL Receptor Extracellular Domain at Endosomal pH, *Science*, 298 (2002) 2353-2358.
- [14] J.E. Murphy, P.R. Tedbury, S. Homer-Vanniasinkam, J.H. Walker, S. Ponnambalam,

Biochemistry and cell biology of mammalian scavenger receptors, *Atherosclerosis*, 182 (2005) 1-15.

[15] Y.I. Miller, M.K. Chang, C.J. Binder, P.X. Shaw, J.L. Witztum, Oxidized low density lipoprotein and innate immune receptors, *Current opinion in lipidology*, 14 (2003) 437-445.

[16] X.P. Chen, T.T. Zhang, G.H. Du, Lectin-like oxidized low-density lipoprotein receptor-1, a new promising target for the therapy of atherosclerosis?, *Cardiovasc Drug Rev*, 25 (2007) 146-161.

[17] M. Chen, T. Masaki, T. Sawamura, LOX-1, the receptor for oxidized low-density lipoprotein identified from endothelial cells: implications in endothelial dysfunction and atherosclerosis, *Pharmacol.Ther.*, 95 (2002) 89-100.

[18] T. Aoyama, M. Chen, H. Fujiwara, T. Masaki, T. Sawamura, LOX-1 mediates lysophosphatidylcholine-induced oxidized LDL uptake in smooth muscle cells, *FEBS Letters*, 467 (2000) 217-220.

[19] N. Kume, T. Kita, Apoptosis of Vascular Cells by Oxidized LDL, *Circulation research*, 94 (2004) 269-270.

[20] N. Inoue, T. Sawamura, Lectin-like oxidized LDL receptor-1 as extracellular chaperone receptor: its versatile functions and human diseases, *Methods*, 43 (2007) 218-222.

[21] K. Inoue, Y. Arai, H. Kurihara, T. Kita, T. Sawamura, Overexpression of lectin-like oxidized low-density lipoprotein receptor-1 induces intramyocardial vasculopathy in apolipoprotein E-null mice, *Circulation research*, 97 (2005) 176-184.

[22] I. Ohki, T. Ishigaki, T. Oyama, S. Matsunaga, Q. Xie, M. Ohnishi-Kameyama, T. Murata, D. Tsuchiya, S. Machida, K. Morikawa, S. Tate, Crystal structure of human lectin-like, oxidized low-density lipoprotein receptor 1 ligand binding domain and its ligand recognition mode to OxLDL, *Structure.(Camb.)*, 13 (2005) 905-917.

[23] T. Ishigaki, I. Ohki, T. Oyama, S. Machida, K. Morikawa, S. Tate, Purification, crystallization and preliminary X-ray analysis of the ligand-binding domain of human lectin-like oxidized low-density lipoprotein receptor 1 (LOX-1), *Acta Crystallogr.Sect.F.Struct.Biol Cryst.Commun.*, 61 (2005) 524-527.

[24] H. Park, F.G. Adsit, J.C. Boyington, The 1.4 angstrom crystal structure of the human oxidized low density lipoprotein receptor lox-1, *Journal of Biological Chemistry*, 280 (2005) 13593-13599.

[25] I. Ohki, H. Amida, R. Yamada, M. Sugihara, T. Ishigaki, S. Tate, Surface plasmon resonance study on functional significance of clustered organization of lectin-like oxidized LDL receptor (LOX-1), *Biochim Biophys Acta*, 1814 (2011) 345-354.

- [26] S. Matsunaga, Q. Xie, M. Kumano, S. Niimi, K. Sekizawa, Y. Sakakibara, S. Komba, S. Machida, Lectin-like oxidized low-density lipoprotein receptor (LOX-1) functions as an oligomer and oligomerization is dependent on receptor density, *Exp Cell Res*, 313 (2007) 1203-1214.
- [27] G. Rudenko, L. Henry, K. Henderson, K. Ichtchenko, M.S. Brown, J.L. Goldstein, J. Deisenhofer, Structure of the LDL receptor extracellular domain at endosomal pH, *Science*, 298 (2002) 2353-2358.
- [28] T. Ishigaki, I. Ohki, N. Utsunomiya-Tate, S.I. Tate, Chimeric structural stabilities in the coiled-coil structure of the NECK domain in human lectin-like oxidized low-density lipoprotein receptor 1 (LOX-1), *J.Biochem.(Tokyo)*. 141 (2007) 855-866.
- [29] Z. Otwinowski, W. Minor, Processing of X-ray diffraction data collected in oscillation mode, in: Charles W. Carter, Jr. (Ed.) *Methods in enzymology*, vol. 276, Academic Press, 1997, pp. 307-326.
- [30] A. Vagin, A. Teplyakov, MOLREP: an Automated Program for Molecular Replacement, *Journal of Applied Crystallography*, 30 (1997) 1022-1025.
- [31] M.D. Winn, An overview of the CCP4 project in protein crystallography: an example of a collaborative project, *J Synchrotron Radiat*, 10 (2003) 23-25.
- [32] G.N. Murshudov, A.A. Vagin, E.J. Dodson, Refinement of macromolecular structures by the maximum-likelihood method, *Acta Crystallogr D Biol Crystallogr*, 53 (1997) 240-255.
- [33] P. Emsley, B. Lohkamp, W.G. Scott, K. Cowtan, Features and development of Coot, *Acta Crystallogr D Biol Crystallogr*, 66 (2010) 486-501.
- [34] F. Delaglio, S. Grzesiek, G.W. Vuister, G. Zhu, J. Pfeifer, A. Bax, NMRPipe: a multidimensional spectral processing system based on UNIX pipes, *J Biomol NMR*, 6 (1995) 277-293.
- [35] B.A. Johnson, R.A. Blevins, NMRView, A Computer Program for the Visualization and Analysis of NMR Data, *J Biomol NMR*, 4 (1994) 603-614.
- [36] S.C. Gill, P.H. von Hippel, Calculation of protein extinction coefficients from amino acid sequence data, *Anal Biochem*, 182 (1989) 319-326.
- [37] S.J. de Vries, M. van Dijk, A.M. Bonvin, The HADDOCK web server for data-driven biomolecular docking, *Nat Protoc*, 5 (2010) 883-897.
- [38] C. Dominguez, R. Boelens, A.M. Bonvin, HADDOCK: a protein-protein docking approach based on biochemical or biophysical information, *J Am Chem Soc*, 125 (2003) 1731-1737.
- [39] R. Fuchs, S. Schmid, I. Mellman, A possible role for Na<sup>+</sup>,K<sup>+</sup>-ATPase in regulating ATP-dependent endosome acidification, *Proceedings of the National Academy of*

Sciences, 86 (1989) 539-543.

[40] N.A. Baker, D. Sept, S. Joseph, M.J. Holst, J.A. McCammon, Electrostatics of nanosystems: Application to microtubules and the ribosome, Proceedings of the National Academy of Sciences, 98 (2001) 10037-10041.

## Figure legends

**Fig. 1. LOX-1 ligand binding domain structure and the basic spine on its surface.** (A) The basic spine consists of the linearly arranged Arg residues, represented in blue spheres, on the ligand binding surface of the CTLD dimer [22]. The basic spine shaded in blue is able to adopt an  $\alpha$ -helix up to 37-residues long. (B) The side-view of LOX-1 dimer shows the positions of the W150 and C140 residues described in the manuscript. In this crystal structure (PDB ID: 1YXK), one of the C140 residues in the homodimer was not detected (marked with n.d.), due to the intrinsic flexibility of that region; the existence of the disulfide bond was confirmed by SDS PAGE and a possible bond position is indicated with a red line [22]. The orange arrow indicates the ligand binding surface harboring the basic spine.

**Fig. 2. Structural comparison of mCTLD<sup>w150a</sup>, mCTLD<sup>wt</sup> and dCTLD<sup>wt</sup> in the canonical dimer.** (A) The backbone structures of mCTLD<sup>w150a</sup> (red) and mCTLD<sup>wt</sup> (blue) were superimposed onto a CTLD from the canonical dimer (gray). The position for W150 is marked with a yellow circle. The letters in parentheses indicates the chain name. (B) The residues in the dimer interface are displayed on a cross section of the canonical dimer. The surface is drawn on the canonical dimer crystal structure of NECK14-CTLD (PDB ID: 1YXK). The structures mCTLD<sup>w150a</sup> (red) and mCTLD<sup>wt</sup> (blue) are superimposed onto a CTLD from the canonical dimer (gray), the chain A, as shown in the above drawings.

**Fig. 3. Inter-domain hydrophobic interactions mediated by W150.** (A) The hydrophobic interactions that embed W150 in the hydrophobic pocket formed by residues P143, C144 and P145 and Q146, which are found in the canonical dimer structure (PDB ID: 1YXK). The letters in parentheses indicate the chain IDs. (B) The corresponding hydrophobic interactions found in the postulated mCTLD<sup>wt</sup> dimer model are superimposed onto a CTLD in the canonical dimer structure. (C) The hydrophobic interactions expected in the plausible mCTLD<sup>w150a</sup> dimer model are superimposed onto the structure of a CTLD in the canonical dimer.

**Fig. 4. Hydrogen bonding mediated by H151.** (A) The inter-domain hydrogen bonding between H151 and D147 in the canonical CTLD dimer structure in the NECK14-CTLD crystal structure (PDB ID: 1YXK). (B) The intra-chain hydrogen bonding between H151

and D187 in the mCTL<sup>D</sup><sup>wt</sup> structure. The model dimer prepared by superimposing the mCTL<sup>D</sup><sup>wt</sup> onto the canonical CTL<sup>D</sup> dimer shows the slight side-chain flip from the original position. (C) The hydrogen bond between H151 and D187 in the mCTL<sup>D</sup><sup>w150a</sup> is embedded in the modeled dimer. In mCTL<sup>D</sup><sup>w150a</sup> structure, the side-chain orientation of D147 had also changed from that in the dCTL<sup>D</sup><sup>wt</sup>.

**Fig. 5. Inter-domain hydrophobic interactions between Y197 and the Phe-cluster.** (A) The additional inter-domain hydrophobic interactions mediated between Y197 and the hydrophobic cluster consisting of Phe-residues F158, F200 and F202. (B) The corresponding interactions found in the model dimer structure with the mCTL<sup>D</sup><sup>wt</sup> protein. The ring orientation of F200 is altered from that observed in the canonical dimer, which appears to block residue Y197 from accessing the Phe-cluster. The Y197 side-chain orientation had changed in the absence of the inter-domain interaction. (C) A similar side-chain flip of F200 observed in the mCTL<sup>D</sup><sup>wt</sup> protein was also found in the mCTL<sup>D</sup><sup>w150a</sup> construct. The observed changes for the side-chains arise because of the absence of the inter-domain interactions found in the canonical dimer.

**Fig. 6. NMR identification of the structurally deformed parts caused by the W150A mutation.** (A) Comparison of the 2D <sup>1</sup>H-<sup>15</sup>N HSQC spectra for the wild-type (black) and W150A (red) CTL<sup>D</sup> fragments comprising residues 143–273. (B) The chemical shift differences (CSDs) observed in comparing the spectra between the wild-type and W150A CTL<sup>D</sup>s. The CSD values were calculated as  $CSD = \sqrt{(\Delta\delta_{HN})^2 + (0.2\Delta\delta_N)^2}$ . The dotted line indicates the value of the average plus one standard deviation of the CSDs. (C) The residues showing the CSD over the value indicated by the dotted line are marked in green on the canonical dimer structure (PDB ID: 1YXK). W150 in both domains is drawn as a stick model.

**Fig. 7. Dimer structures generated by the docking calculations.** (A) The representative reconstructed dimer using dCTL<sup>D</sup><sup>wt</sup> structures by docking calculations with the program HADDOCK with the assumption that residues P143, C144, P145, Q146 and W150 are in contact with each other. The CTL<sup>D</sup>s in the calculated dimer are drawn in salmon and purple. The residues assumed to be in contact in the HADDOCK calculation are shown as space filling atom models. The structure in gray is the canonical dimer crystal structure of the NECK14-CTL<sup>D</sup> (PDB ID: 1YXK), on which the calculated dimer structure is superimposed. (B) The most probable dimer model obtained by the

HADDOCK calculations using the structure of mCTL<sup>D</sup><sub>w150a</sub>. (C) The second most probable structure from the HADDOCK calculation using the mCTL<sup>D</sup><sub>w150a</sub> coordinates. Each right-hand side structure is the view seen from the direction indicated by an arrow in the left-hand side structures. All figures were prepared by the program PyMol ver. 1.2 (Schrodinger LLC).

**Fig. 8. Charge distributions on the modeled dimer surfaces.** (A) The reconstructed canonical dimer structure with dCTL<sup>D</sup><sub>wt</sub> determined by the HADDOCK calculation drawn in ribbons (left) and the corresponding surface structure with charge distributions (right). (B) The most probable dimer structure made of mCTL<sup>D</sup><sub>w150a</sub> by the HADDOCK calculation and its surface charge distribution. (C) The second most probable mCTL<sup>D</sup><sub>w150a</sub> dimer from the HADDOCK calculation and its surface charge distribution. All structures are displayed to keep the chain A in the same viewing angles to compare the relative domain arrangement; in the ribbon representations (left), chain A and B are drawn in white and light blue, respectively. All figures were prepared by the program PyMol.ver. 1.2 (Schrodinger LLC). The electrostatic surface potentials were calculated by using the APBS plug-in tools in PyMol [40]; colored from  $-5$  kT/e (red) to  $+5$  kT/e (blue), where  $k$  is the Boltzmann constant,  $T$  is the absolute temperature and  $e$  is the charge of an electron.

**Fig. 9. Schematic drawings to represent the inter-domain interactions of the CTL<sup>D</sup> dimers.** (A) The inter-domain interactions observed in the canonical CTL<sup>D</sup> dimer structure. The tight inter-domain hydrophobic interactions mediated by the W150 ring, which forms a trunk-like structure, stabilize the canonical dimer with associating interactions by H151 and Y197. The inter-chain disulfide bond at C140 is in a relatively flexible part. Therefore, the disulfide bond *per se* does not stabilize the dimer but confines the domains in a limited space to facilitate dimer formation by the self-association feature of the wild-type CTL<sup>D</sup>. The coiled-coil dimer NECK domain is also involved in locating the CTL<sup>D</sup>s in a spatial proximity. The stable canonical dimer maintains the basic spine on its surface (bottom). (B) The W150A mutation loosens the inter-locked hydrophobic contact found in the wild-type canonical dimer, the trunk contact. The lack of the key contact may result in various dimer arrangements showing different surface structures, thus breaking the basic spine (bottom). The existence of the disulfide bond and coiled-coil NECK make the CTL<sup>D</sup>s stay in a spatial proximity. However, the loss of the key inter-domain interaction prohibits the canonical dimer formation but causes relatively random arrangements of the CTL<sup>D</sup>s.

## **Supplementary Materials**

Structural implication for the impaired binding of W150A mutant LOX-1 to oxidized low density lipoprotein, OxLDL

Shogo Nakano, Mamoru Sugihara, Risato Yamada, Katsuo Katayanagi and Shin-ichi Tate\*

## Supplementary figure legends

**Fig. S1. Human LOX-1 domain structure and the fragments used in this work.** TM stands for the trans-membrane domain. CTLD is the C-type lectin-like domain that functions as a ligand binding domain. Thick black bars indicate the locations of the disulfide bonds in the CTLD.

**Fig. S2. Sample elution profile of the gel-filtration chromatography step used to purify the W150A CTLD that was subsequently used in the crystallization process.** The mark 'd' denotes the disulfide-linked dimer of the W150A CTLD, whereas 'm' indicates the peak for the monomeric W150A CTLD. The reduced ability of the W150A CTLD to self-associate meant that the majority of the sample was in the monomeric form following the refolding step. This was in contrast to the wild-type CTLD, which eluted from the column predominantly as a disulfide-linked dimer. The fractions containing monomeric mCTLD<sup>w150a</sup> were subjected to crystallization.

**Fig. S3. Crystal structures for the wild-type CTLD.** (A) The dimer crystal structure for the CTLD fragment (residues 143–273), PDB code 1YXJ. W150 is drawn as a stick presentation. Two molecules of ethylene glycol are sandwiched by the CTLDs. (B) The inter-domain hydrophobic interactions observed in the canonical dimer obtained for the NECK14-CTLD fragment, residues 129–273, (PDB code 1YXK). The ring moiety of W150 is embedded in the hydrophobic clusters formed by the residues P143, C144, P145 and P146. (C) The bottom view of the hydrophobic residues engaged in forming the canonical dimer. The hydrophobic residues form a trunk-like structure.

**Fig. S4. The different domain arrangements in the modeled dimers from the canonical dimer structure.** (A) The structure of the NECK14-CTLD canonical dimer (PDB code 1YXK): the structure in the right is the same structure in the left rotated along the arrow by 90 deg. (B) The most probable HADDOCK model dimer structure of mCTLD<sup>w150a</sup>, displayed with the chain A (gold) overlaid onto the corresponding chain in the wild-type NECK14-CTLD canonical dimer: the chain B for the wild-type and W150A mutant are colored in gray and cyan, respectively. (C) The second probable HADDOCK model dimer of mCTLD<sup>w150a</sup> with the chain A (gold) overlaid to that in the wild-type canonical dimer. The chain B in the model dimer is colored in light blue.

**Fig. S5. Dimerization assays for assessing the self-assembly of NECK10-CTLDS.** (A) Self-assembly of the wild-type NECK10-CTLD was confirmed by observing the disulfide-linked dimer. The ability of the wild-type protein to self-assemble was reduced under acidic conditions, as based on the reduced amount of the disulfide-linked dimer. The W150A mutant NECK10-CTLD did not give significant amounts of the disulfide-linked dimer, indicating that this construct has significantly reduced ability to self-associate. (B) The bands appearing at the higher molecular weight positions were confirmed to be the disulfide-linked dimer, as these bands disappeared following treatment of the sample with  $\beta$ -mercaptoethanol.

**Table 1**Data collection statistics for W150A LOX-1 CTLD, mCTLD<sup>w150a</sup>

Crystal data	
crystallization pH	5.0
Space group	P4 <sub>1</sub> 2 <sub>1</sub> 2
Unit-cell parameters	
a (Å)	62.24
b (Å)	62.24
c (Å)	76.67
Data collection	
Wavelength (Å)	0.9
Resolution (Å)	38–2.3
Reflections	98171
Unique reflections	7061
Completeness (%)	97.3 (95.5)
I/σ(I)	45.8 (10.9)
R <sub>sym</sub> <sup>a</sup>	0.094 (0.369)
B from Wilson plot (Å <sup>2</sup> )	33.8
Refinement	
R <sup>b</sup>	0.182
R <sub>free</sub> <sup>c</sup>	0.246
Rmsd bond length (Å)	0.022
Rmsd bond angle (deg.)	1.815
chiral volume (Å <sup>3</sup> )	0.139
PDB ID	3VLG

<sup>a</sup>  $R_{\text{sym}} = \sum_h \sum_i |I_i(h) - \langle I(h) \rangle| / \sum_h I(h)$ , where  $I_i(h)$  is the  $i$ th measurement of reflection  $h$ , and  $\langle I(h) \rangle$  is the mean value of the symmetry related reflection intensities. Values in brackets (2.38–2.30 Å) are for the shell of the highest resolution.

<sup>b</sup>  $R = \sum ||F_o| - |F_c|| / \sum |F_o|$ , where  $F_o$  and  $F_c$  are the observed and calculated structure factors used in the refinement, respectively.

<sup>c</sup>  $R_{\text{free}}$  is the  $R$ -factor calculated with 5% of the reflections chosen at random and omitted from the refinement.

**Table 2**HADDOCK docking parameters<sup>a</sup>

	Wild-type CTLD	W150A CTLD
HADDOCK score	-116.5 ± 1.9	-71.5 ± 3.1
Cluster size	71	93
RMSD <sup>b</sup>	0.9 ± 0.6	7.6 ± 0.4
Van der Waals energy	-71.7 ± 7.4	-49.0 ± 4.1
Electrostatic energy	-90.8 ± 24.3	-99.7 ± 20.1
Desolvation energy	-27.9 ± 2.2	-2.7 ± 5.7
Restraints violation energy	12.2 ± 4.56	0.6 ± 0.56
Buried surface area	1837.5 ± 62.6	1215.4 ± 37.3

<sup>a</sup> The parameters are estimated for the structures in the most probable cluster according to the HADDOCK criteria.

<sup>b</sup> Root mean square deviations of the backbone atoms from the overall lowest-energy structure.

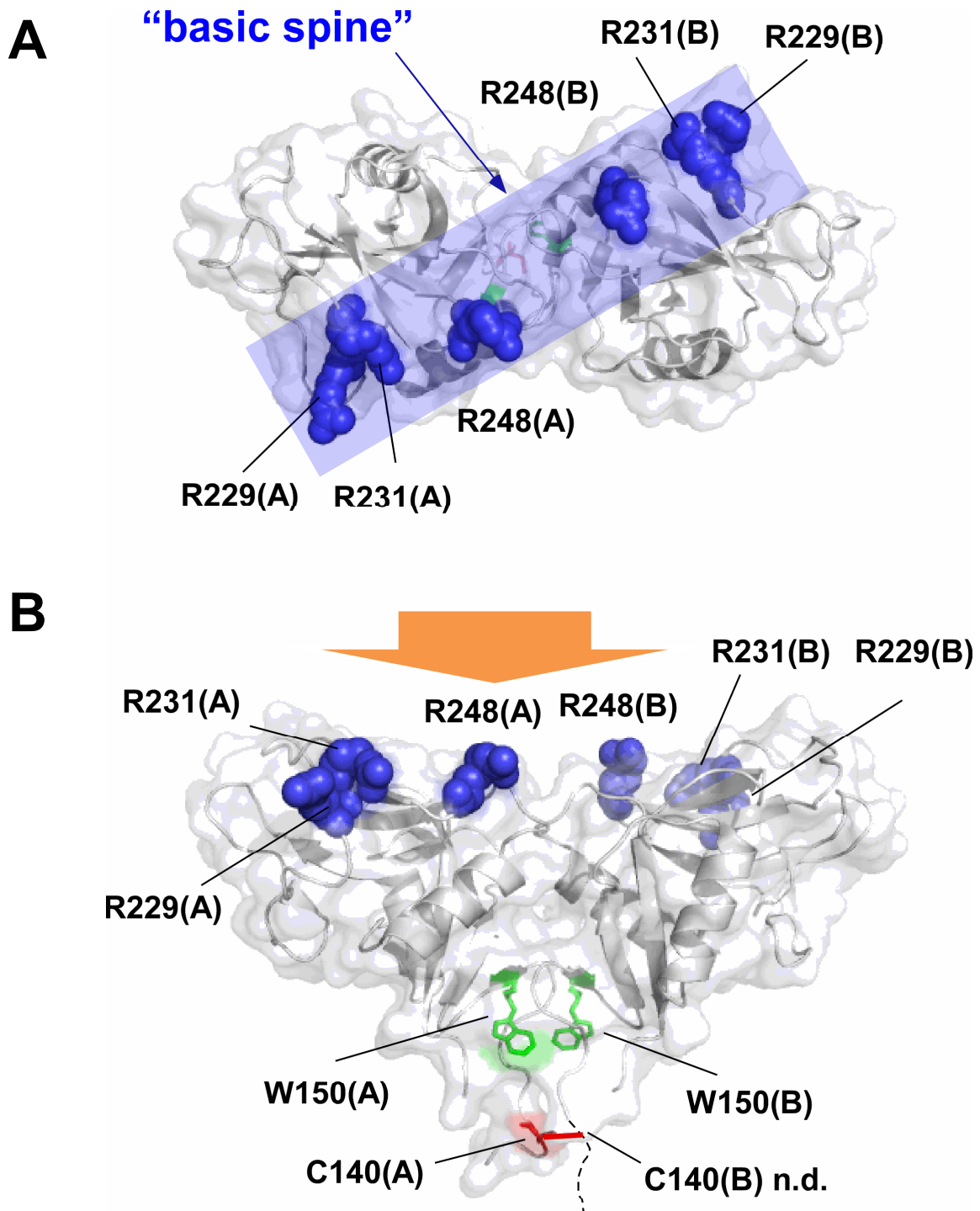


**Fig. 1**

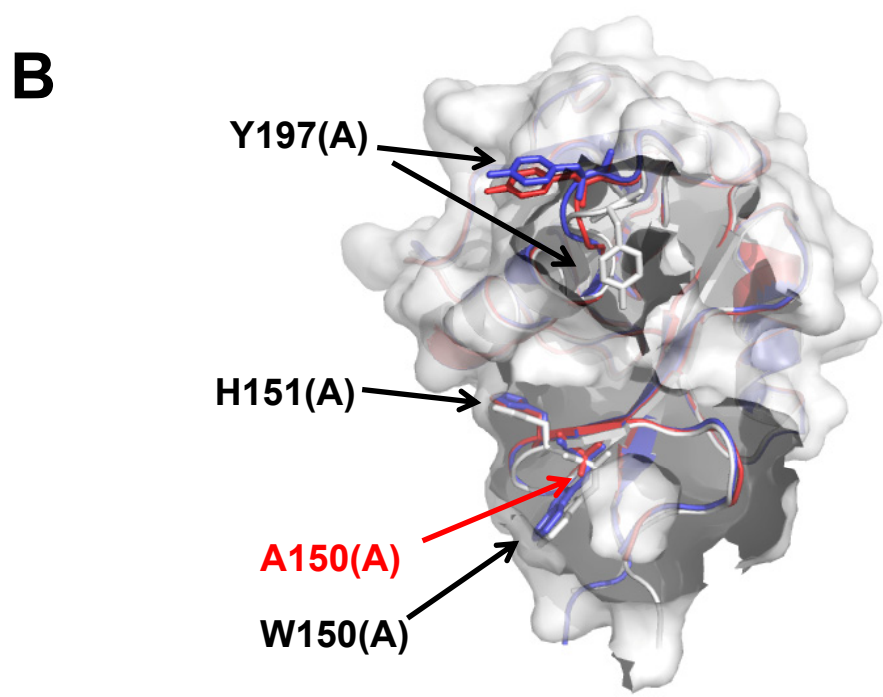
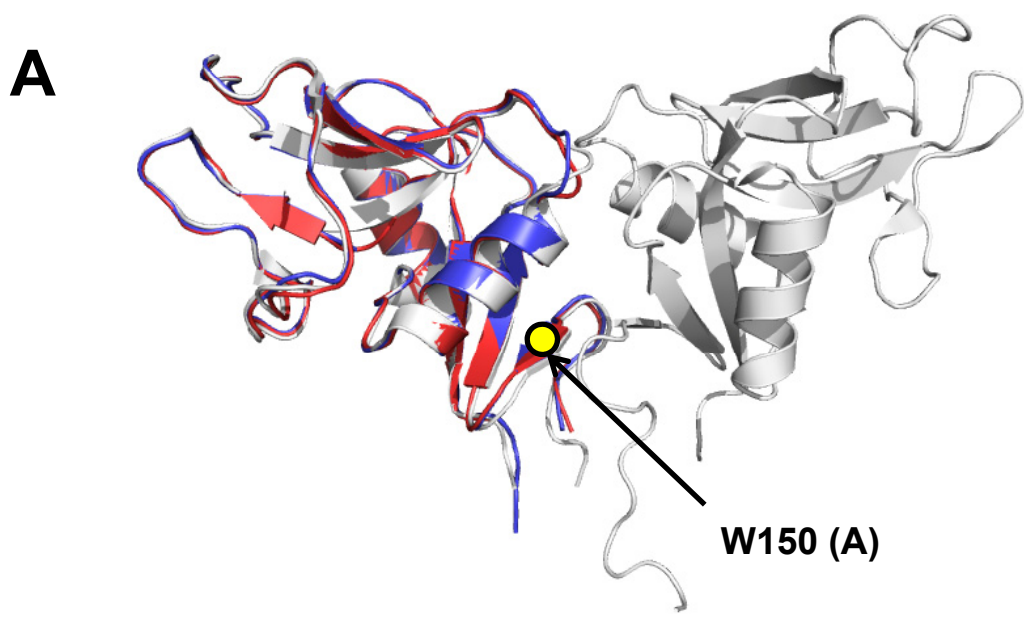


**Fig. 2**

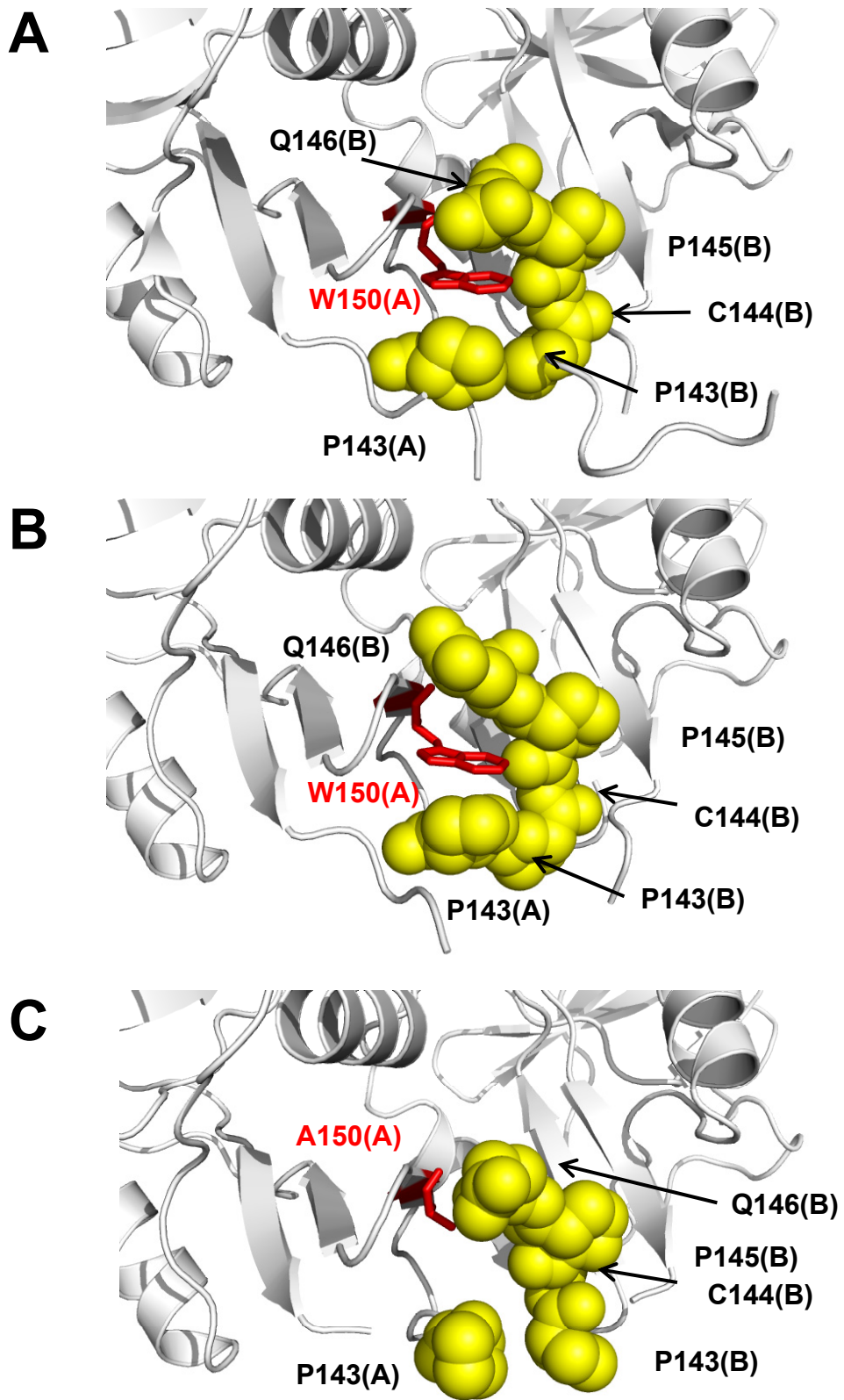


**Fig. 3**

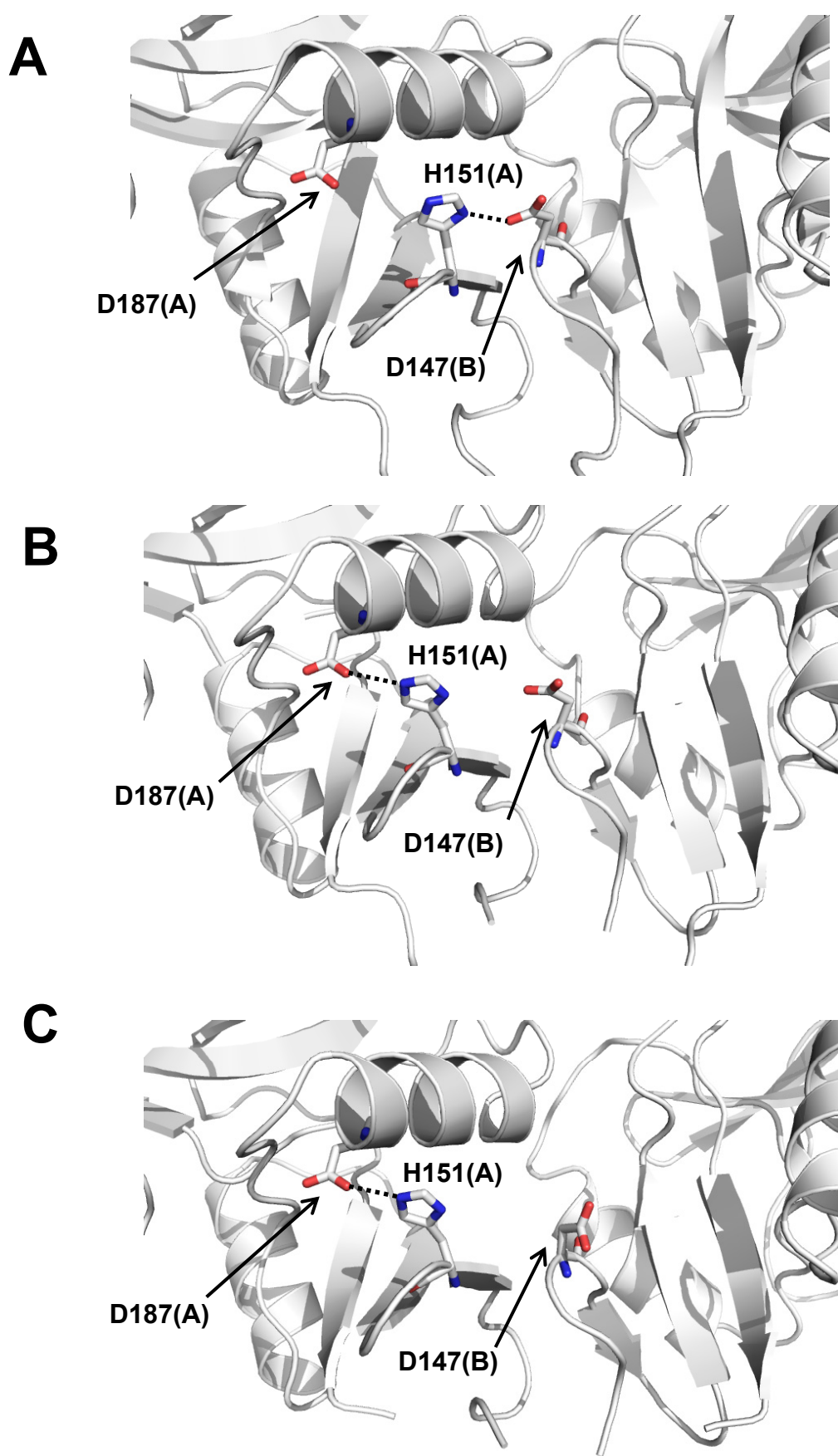


**Fig. 4**

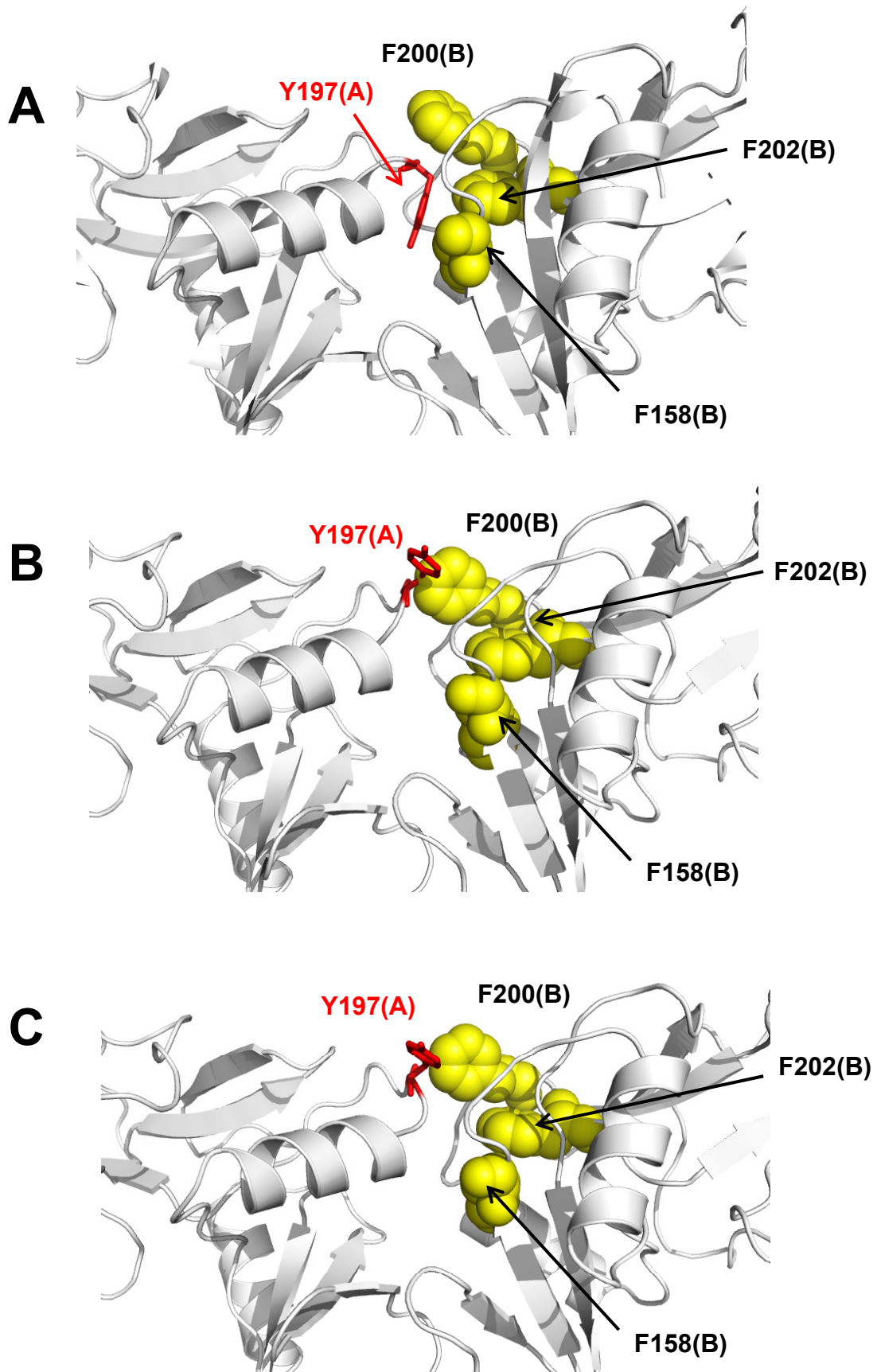


**Fig. 5**

A

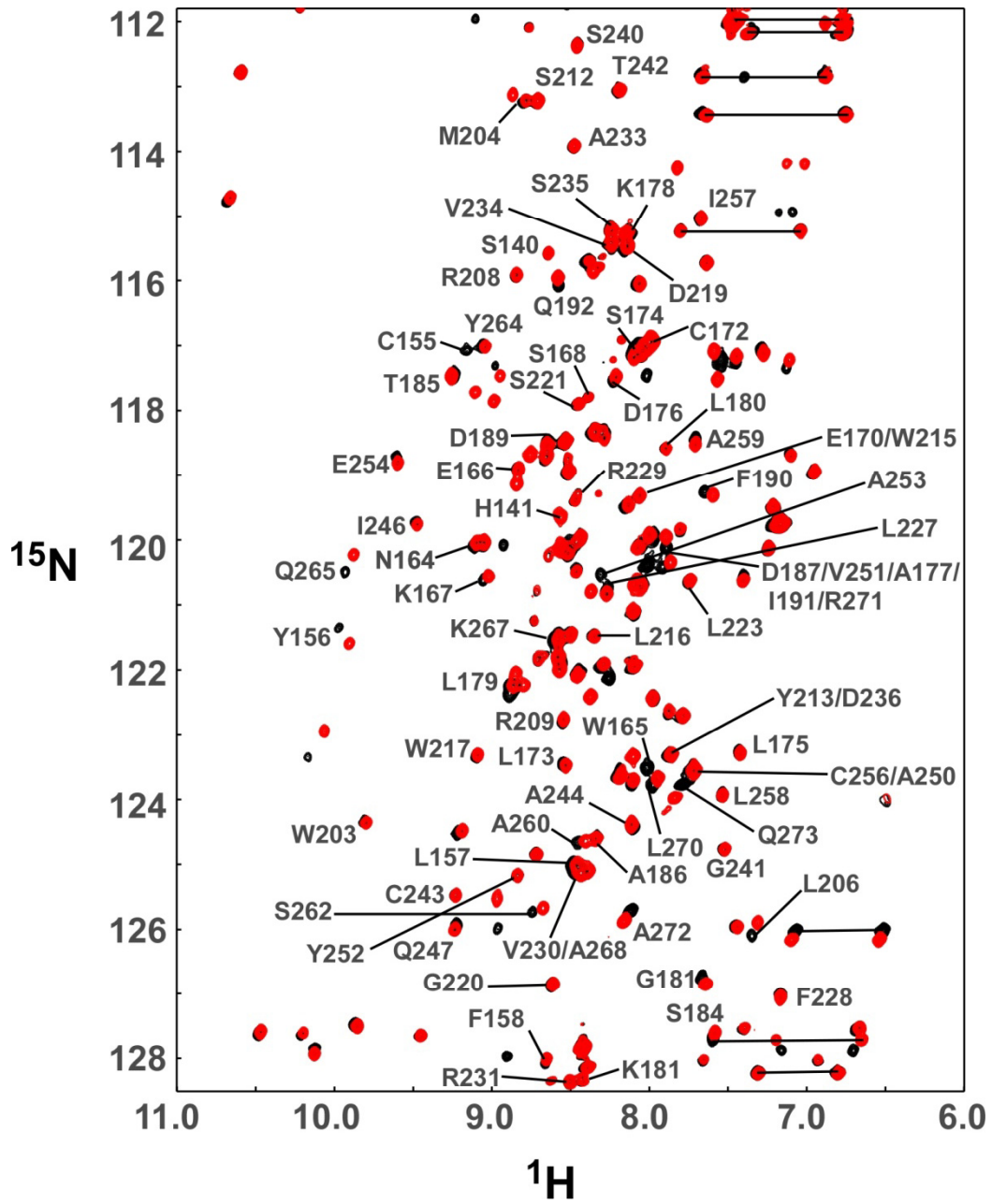
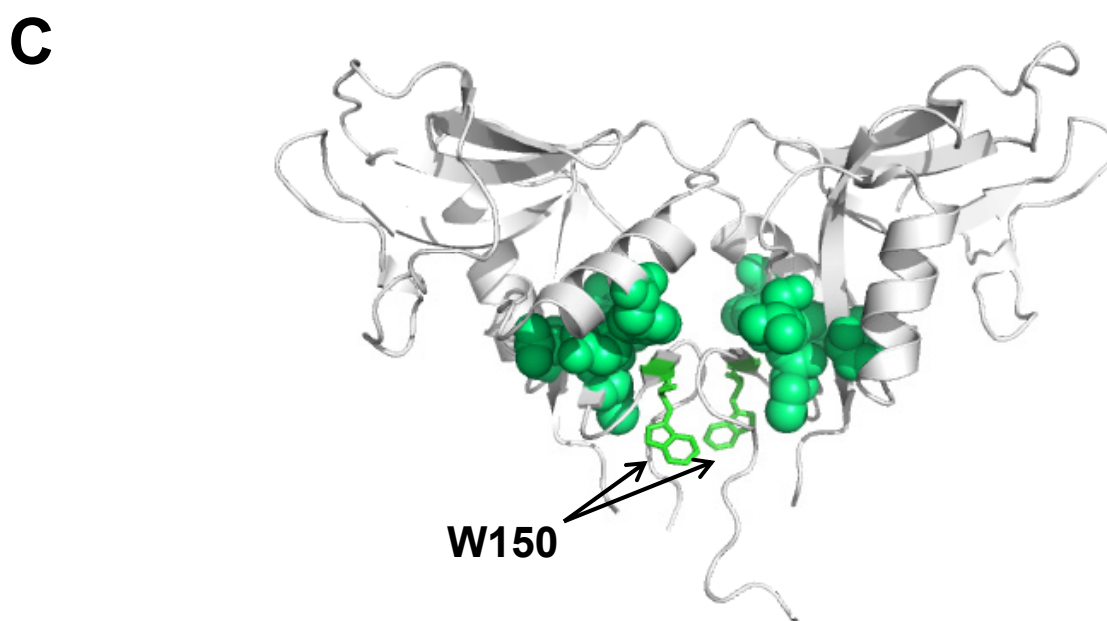
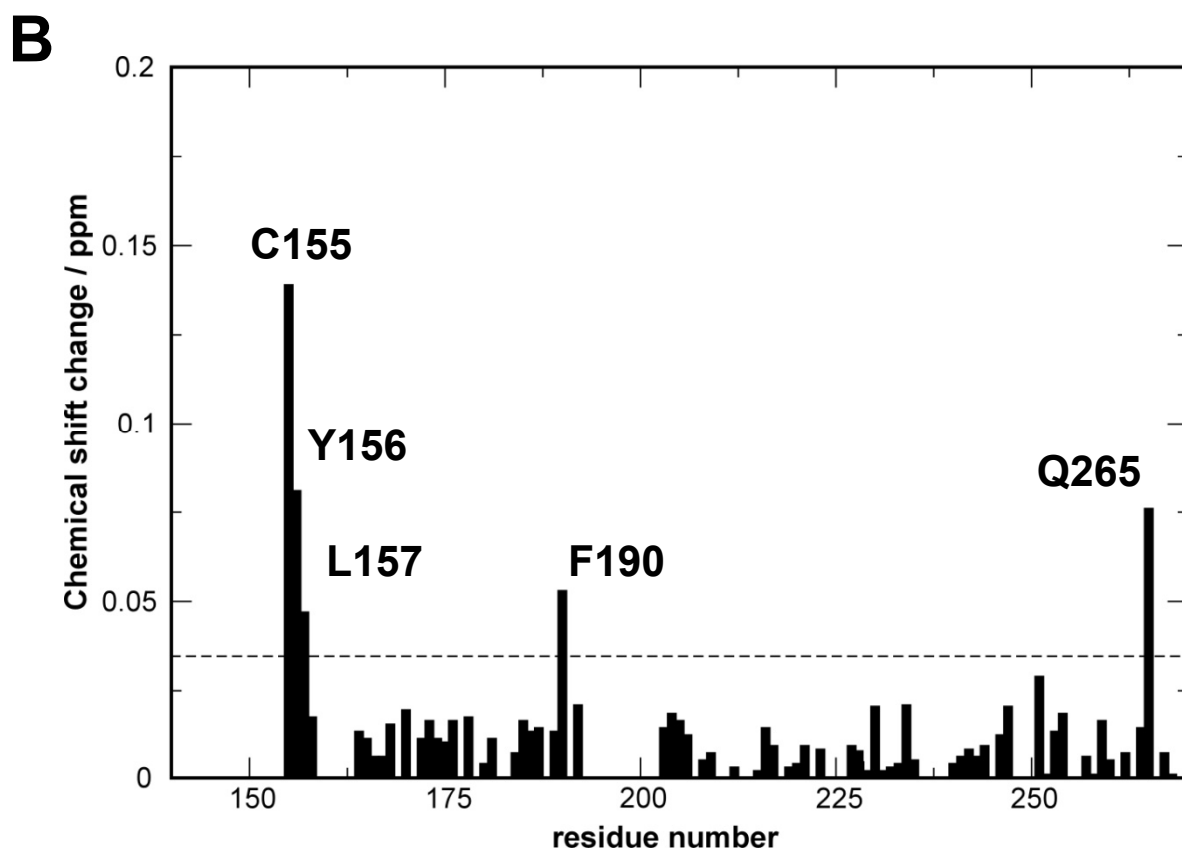
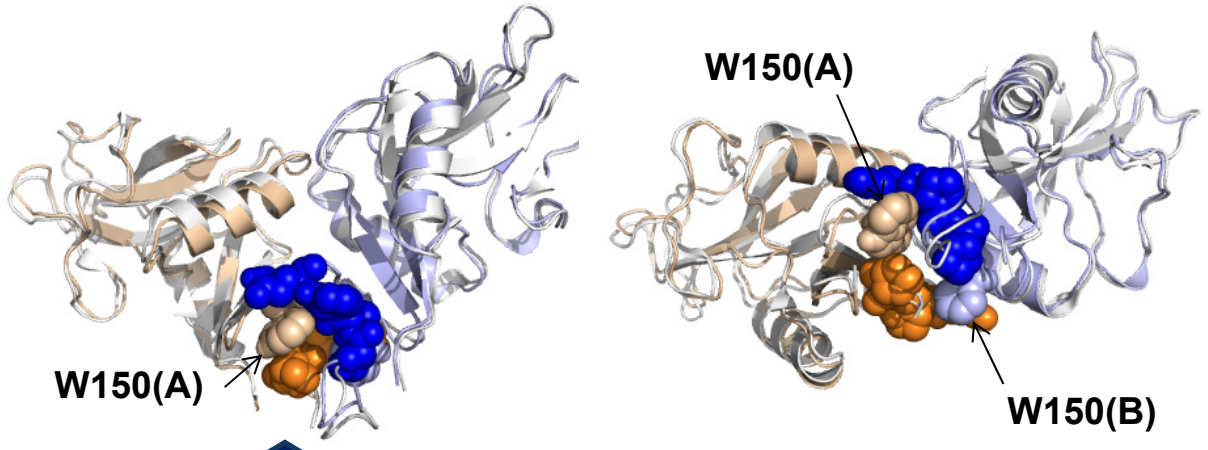


Fig. 6

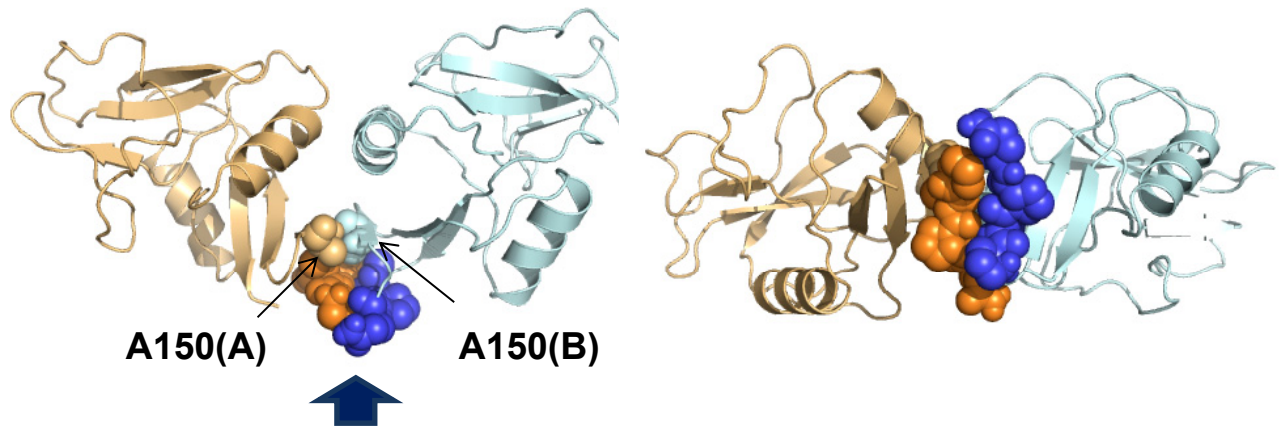


**Fig. 6**

**A**



**B**



**C**

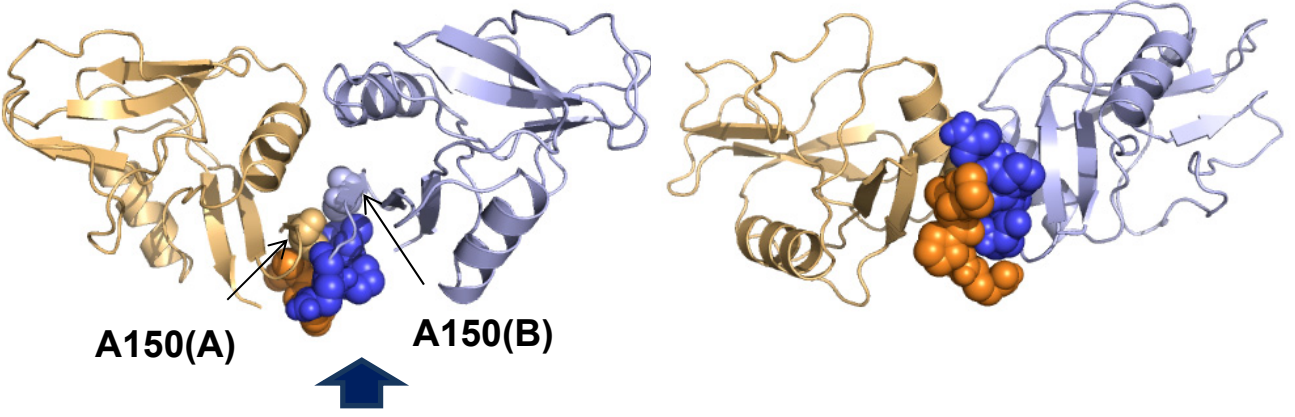
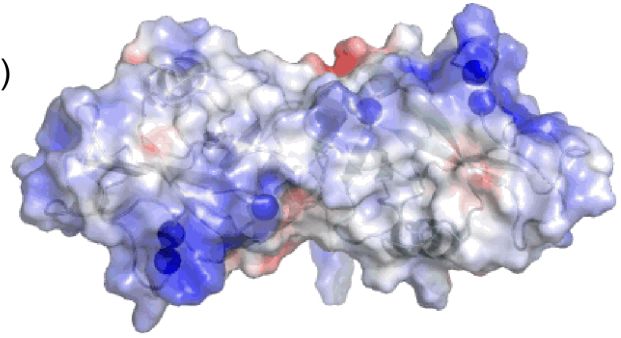
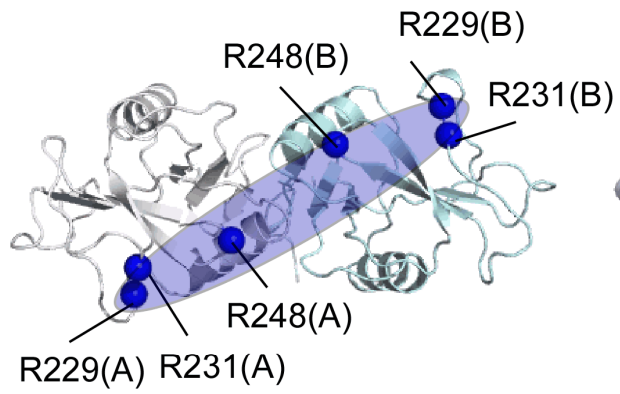
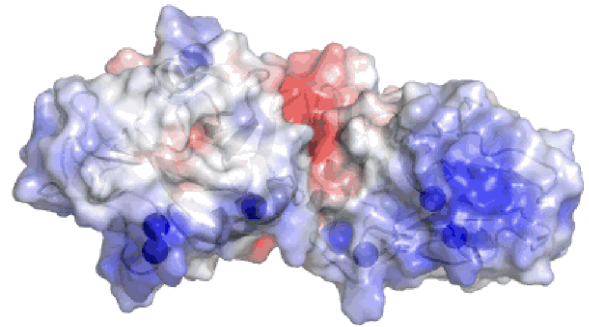
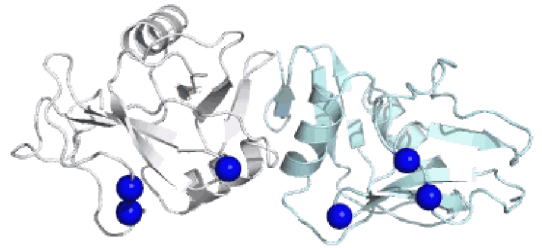


**Fig. 7**

**A**



**B**



**C**

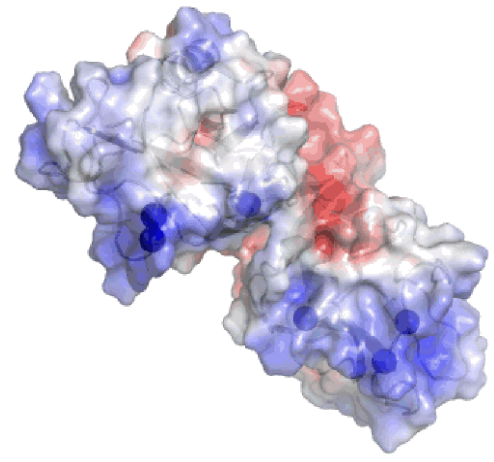
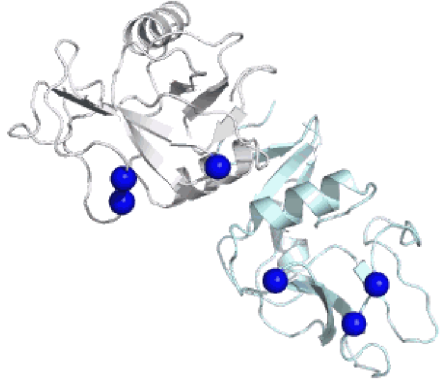


**Fig. 8**

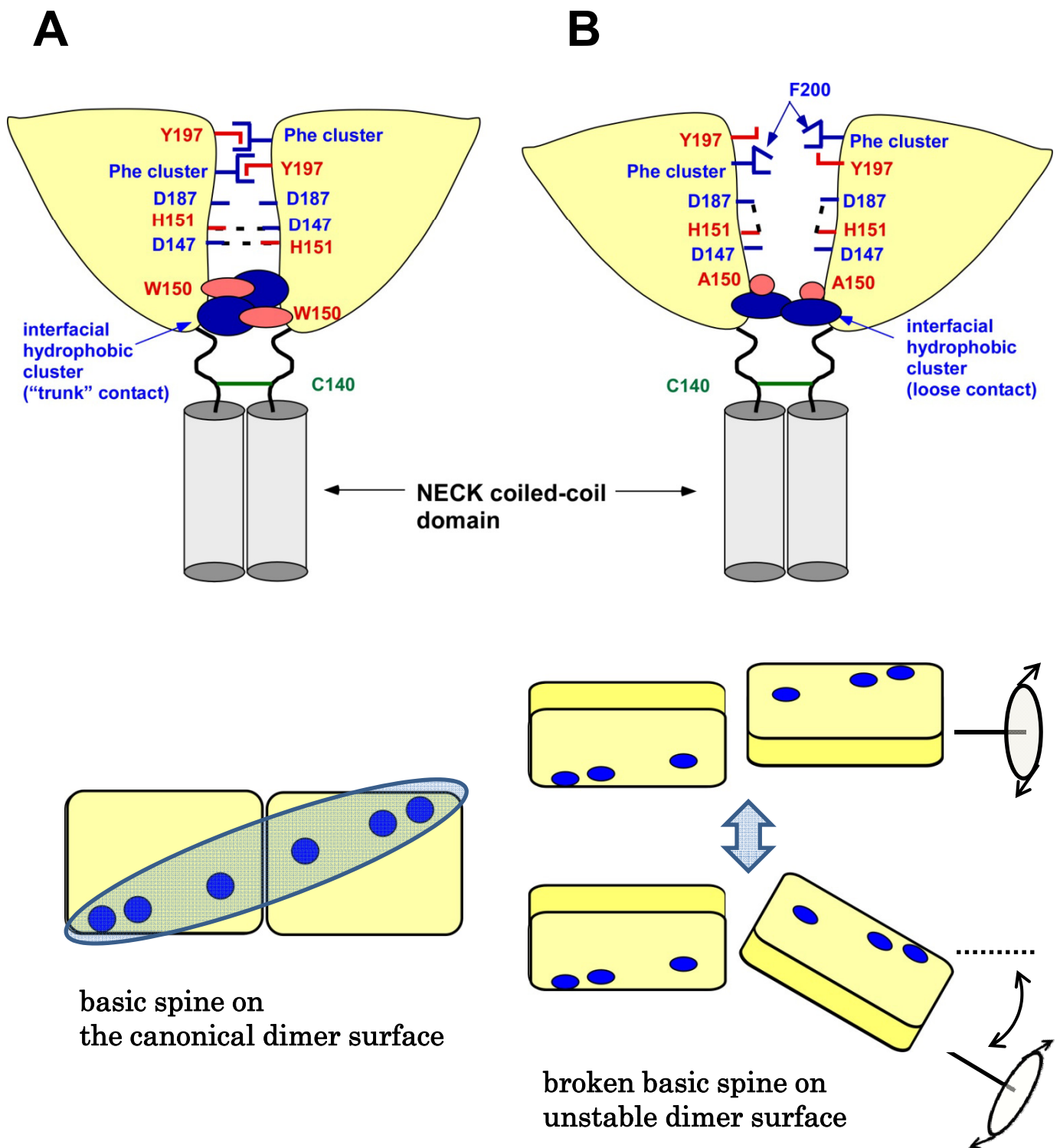


**Fig. 9**

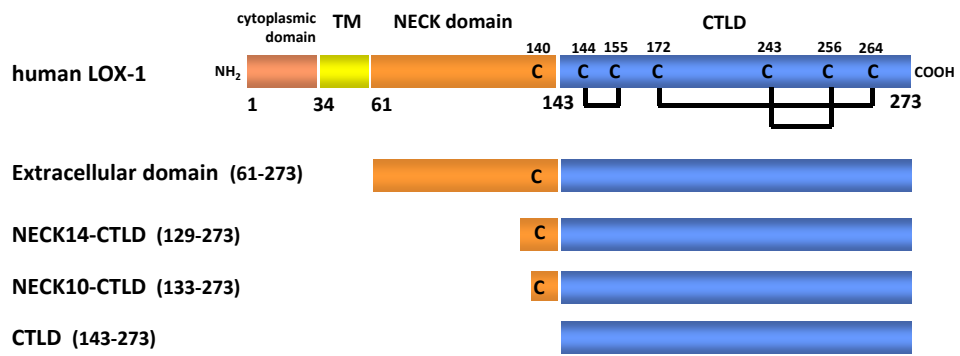


**Fig. S1**

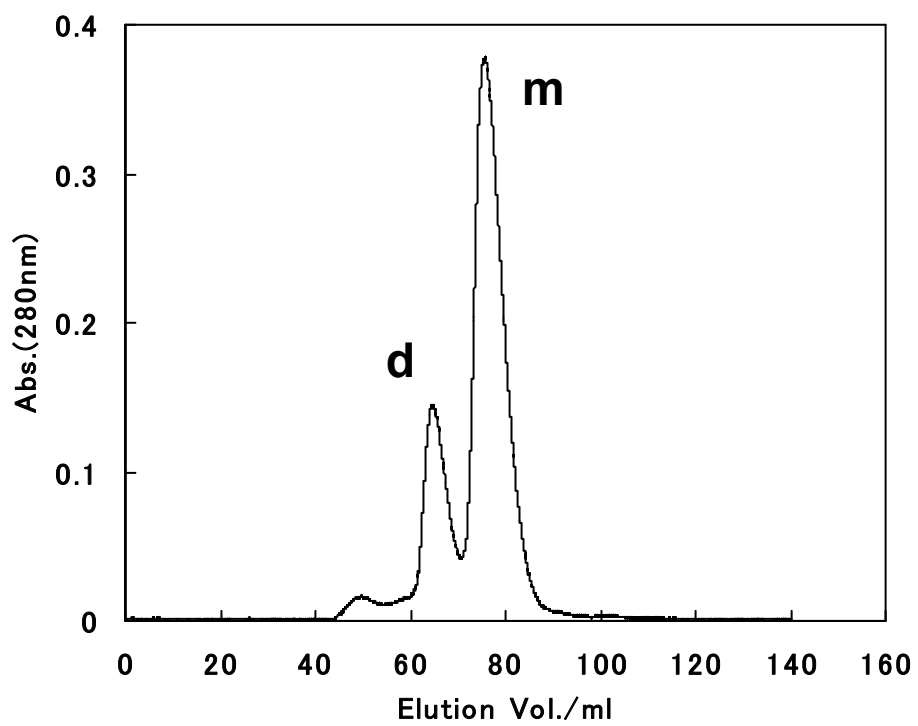
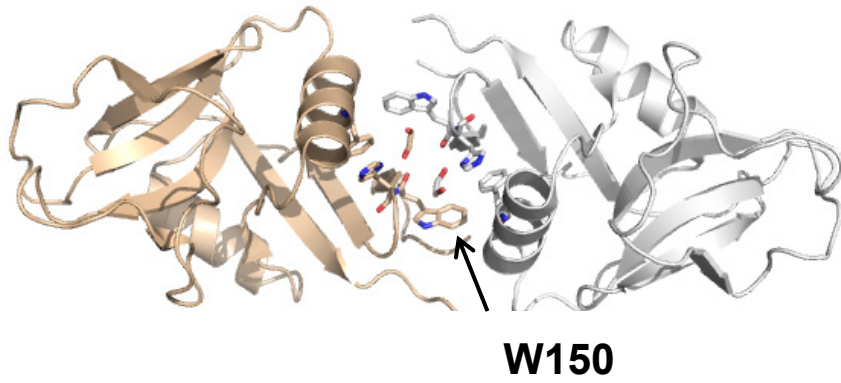
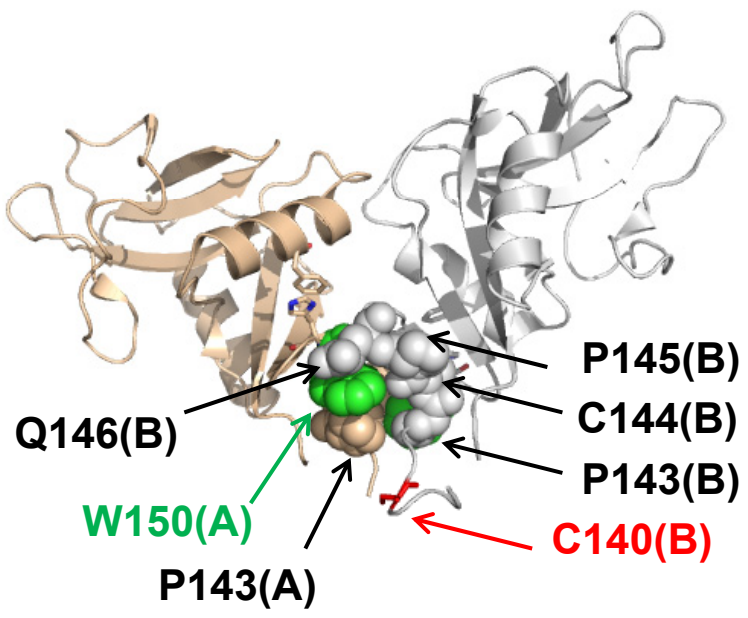


**Fig. S2**

**A**



**B**



**C**

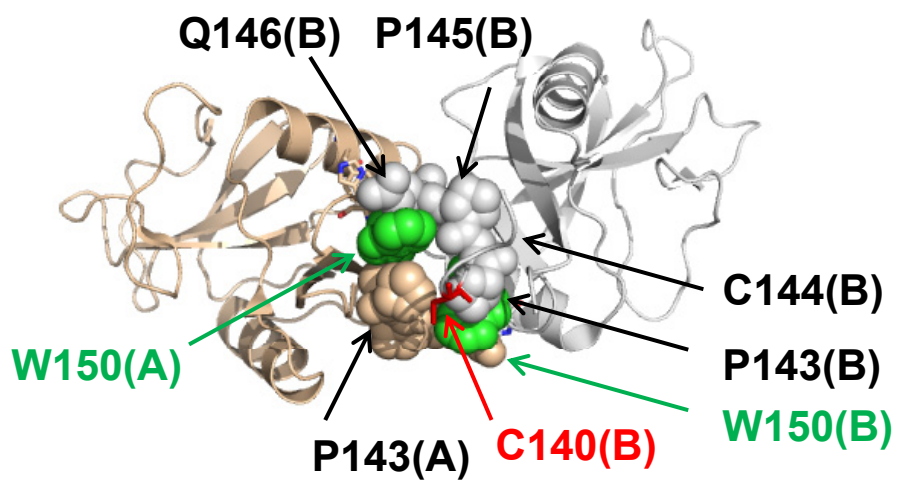
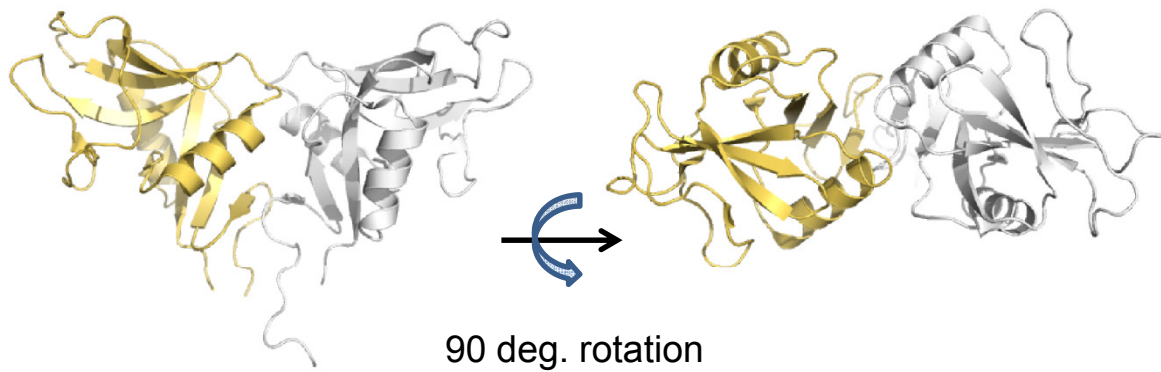
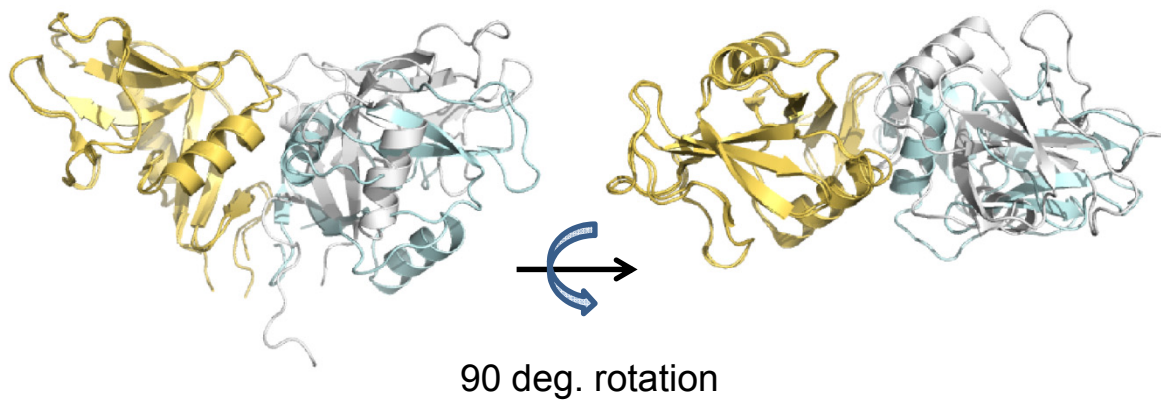


**Fig. S3**

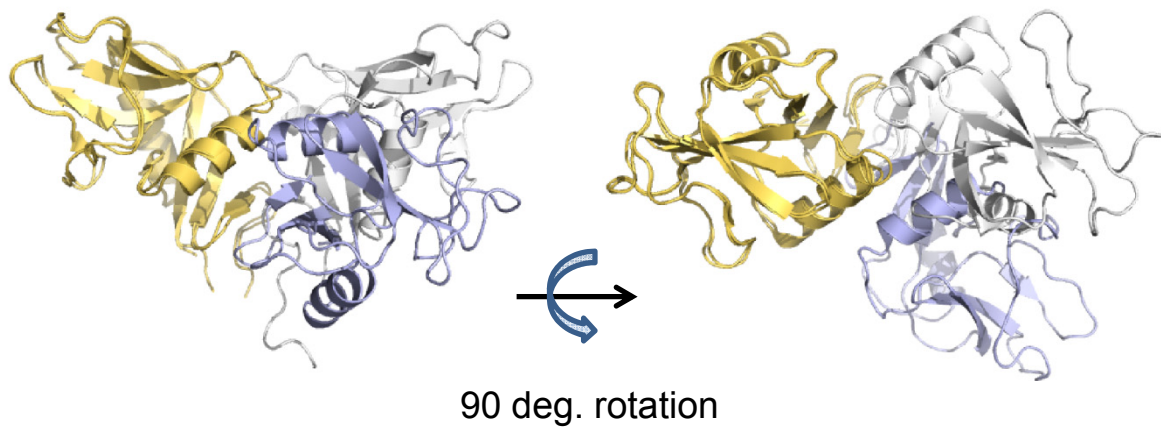
**A**



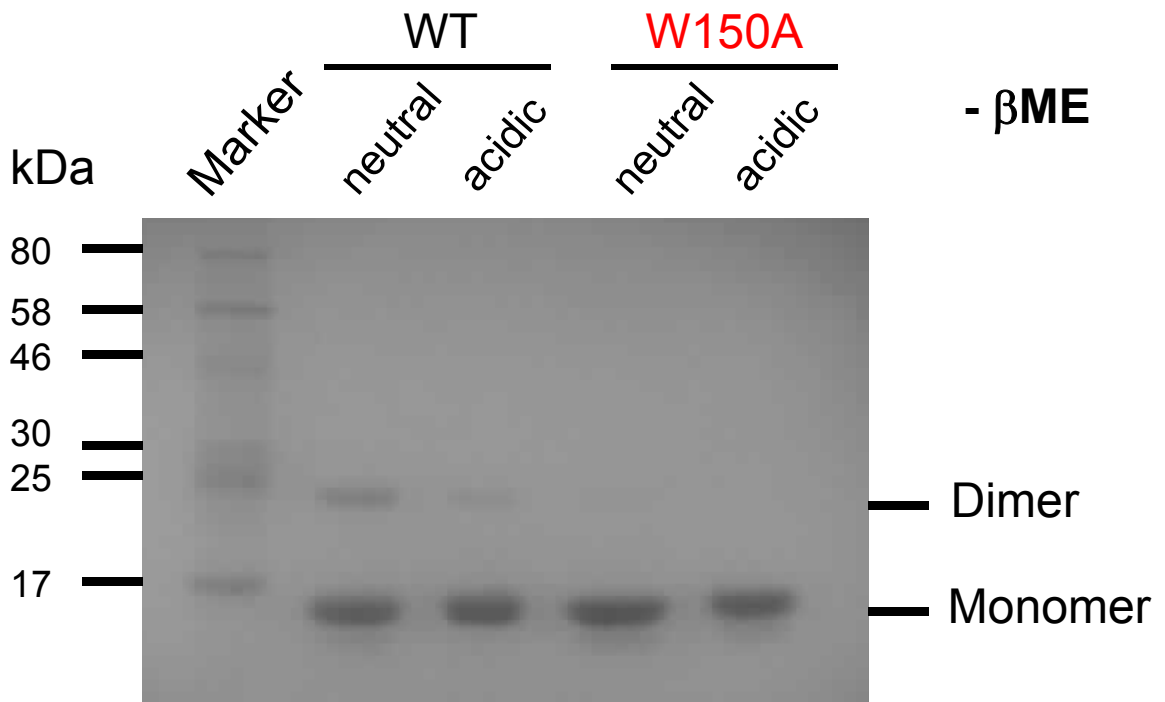
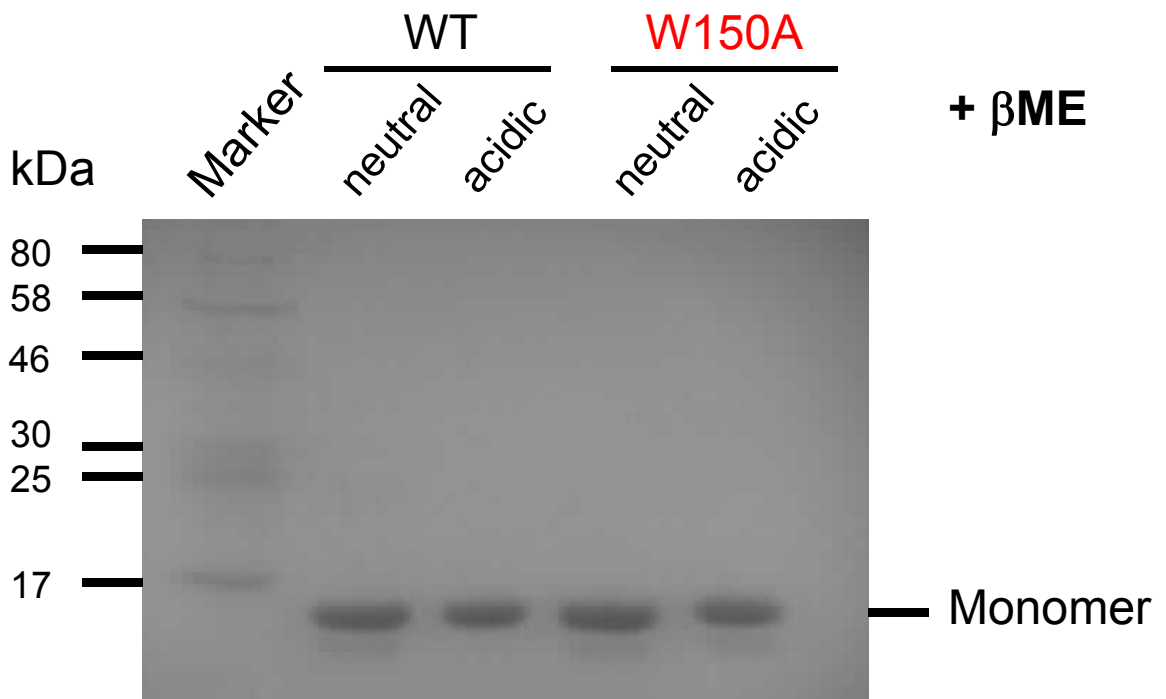
**B**



**C**



**Fig. S4**

**A****B****Fig. S5**